

Advances in Organic Photovoltaic Cells: Fine-Tuning of the Photovoltaic Processes

Morongwa E. Ramoroka,* Sodiq T. Yussuf, Kelechi C. Nwambaekwe,
Kwena D. Modibane, Vivian S. John-Denk, Samantha F. Douman,*
and Emmanuel I. Iwuoha*

This work highlights recent advancements in how the structures and chemical makeups of the active layer materials affect photovoltaic processes and performance in terms of power conversion efficiency and stability. It further sheds light on the performance optimization of organic photovoltaic cell (OPV) and the relationship between these optimization conditions and OPVs performance. The use of different substituents on the same donor or acceptor material has different optimal conditions. Furthermore, it is shown that the addition of different third components in the active layer has different optimal concentration points. This review also highlights and suggests a possible way to improve the stability of OPV through modification of the active layer. To date, some studies showed that incorporation of the third component in the active layer leads to over 97% stability after more than 1000 h.

easily tuned by introduction of substituent and use of different central fused or conjugated core.^[4–7] Inorganic materials for photovoltaic applications can only be modified by replacing a metal with different metals, which may either increase the toxicity of the material or form a more complex crystal structure with possible high concentration of defects.^[8–10] Modified organic materials make it complicated for researchers as they require new optimization conditions. Therefore, it is very important to understand how introduction of a substituent and modification of a central core will affect the properties of organic materials.

The main component of third-generation OPVs is the active layer, which is composed of a blend of electron acceptor

and electron donor materials. Developing new electron donor and acceptor components is an important way to success of OPVs. Currently, the state-of-the-art of the OPVs reached over 19%.^[11,12] Development of new active layer materials and optimization of their OPVs remains important for further improving the performance of OPVs. The operational mechanism of OPVs indicates that to improve the PCE, the design of efficient acceptor and donor materials should consider the following: achieve broad absorption spectra after blending to adequately absorb the incident light for further increase in short-circuit current density (J_{SC}), have adequate E_{LUMO} and E_{HOMO} energy offsets between the acceptor and donor materials to allow charge dissociation, increase the E_{HOMO} of donor and E_{LUMO} of acceptor to improve the open-circuit voltage (V_{OC}), control the blend morphology to ensure sufficient charge transportation, and suppressed electron–hole recombination to enhance the fill factor (FF).^[13,14] Combining electron–donor unit and electron–acceptor unit to form donor–acceptor-based molecules has demonstrated its effectiveness and has been widely used to construct high-performing active layer materials. Donor–acceptor-based molecules are cornerstone of high-performing OPVs through their constant structural modifications.^[15]

From the organic donor and acceptor modifications point of view, introduction of side-chain groups effectively helps in fine-tuning blend film morphology, intermolecular interactions, and regulating crystallinity.^[16–18] It is important to make a good choice of side chain size, position of the substitution, and composition of the side chain.^[19,20] These choices have strong effect on the PCE by controlling the aggregation characteristics of the

1. Introduction

Organic photovoltaic cells (OPVs) have fascinated significant research attention recently because of their advantages such as flexibility, low cost, simple preparation process, and lightweight.^[1–3] In the past five years, the design of new organic materials and optimization of OPVs resulted in a dramatic increase in power conversion efficiency (PCE). In contrast with inorganic counterparts, the properties of organic materials can be

M. E. Ramoroka, S. F. Douman

Department of Chemistry

University of Cape Town

Rondebosch, Cape Town 7707, South Africa

E-mail: rmmr001@myuct.ac.za; samantha.douman@uct.ac.za

M. E. Ramoroka, S. T. Yussuf, K. C. Nwambaekwe, V. S. John-Denk, E. I. Iwuoha

SensorLab (UWC Sensor Laboratories)

University of the Western Cape

4th Floor Chemical Sciences Building, Robert Sobukwe Road, Bellville, Cape Town 7535, South Africa

E-mail: eiwuoha@uwc.ac.za

K. D. Modibane

Department of Chemistry

School of Physical and Mineral Science

University of Limpopo

Sovenga, Polokwane 0727, South Africa

 The ORCID identification number(s) for the author(s) of this article can be found under <https://doi.org/10.1002/solr.202300982>.

DOI: 10.1002/solr.202300982

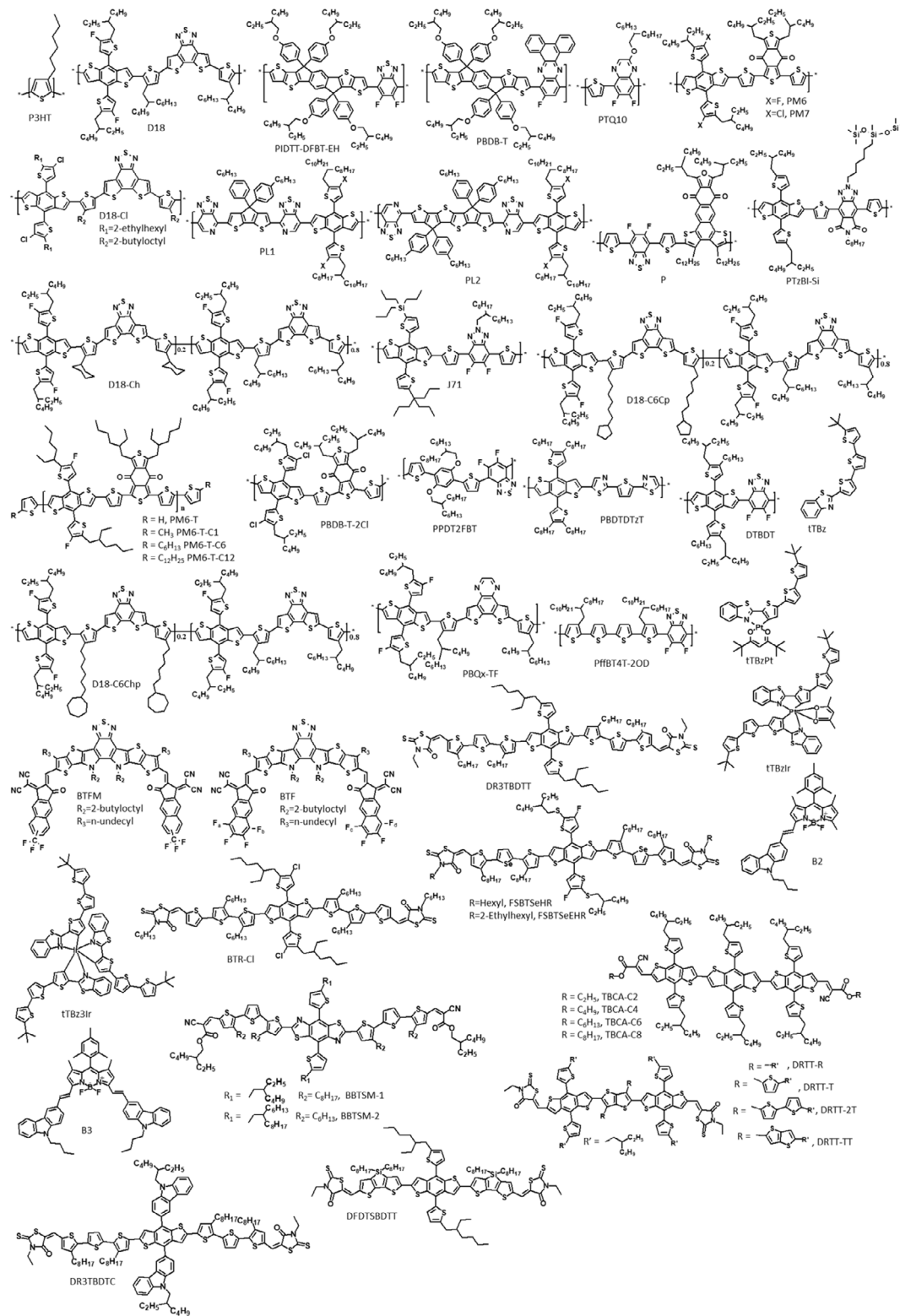
active layer, but structural changes do not guarantee improvement in OPVs performance. Use of more branched or longer alkyl side chains promotes solubility and larger domains size. It is anticipated that materials with larger domain size would have poor charge mobility caused by looser intermolecular packing.^[21] Hu et al.^[22] synthesized novel quinoxaline-based polymer donor with n-octyl and isoocetyl side chains on the quinoxaline unit. In comparison with isoocetyl substituted donor polymer, n-octyl substituted donor polymer demonstrated better molecular packing and stronger intermolecular interactions. After blending with acceptor material, n-octyl substituted donor polymer containing blend displayed efficient electron–hole dissociation, preferable phase separation, better molecular stacking properties, and higher charge mobility with the highest PCE of 17.04%. Zeng et al.^[23] reported two new donor materials synthesized from alkylthiophene benzodithiophene as donor unit along with thiophene and benzene functionalized ester side chains based on quinoxaline as acceptor units. The donor material modified with ester-engineered benzene side chains showed higher hole mobility and stronger intermolecular interaction. After mixing with acceptor polymer, the blend of donor material modified with ester-engineered benzene side chains exhibited balanced hole/electron mobility, reduced charge recombination, better favorable aggregation morphology, and champion PCE of 10.17%. These studies indicate that side-chains engineering method can be effective to improve the PCE of OPVs. Besides branched and linear alkyl chains, studies revealed that cyclo-alkyl chains holds both rigid cyclic part and flexible part, which influence properties of materials, such as increase in intermolecular interactions to adjust self-assemble characteristics and control of steric hindrance to allow charge transportation.^[24] Introduction of substituents on either donor or acceptor material is considered the best way to optimize the morphology of OPVs to elevate the overall performance.

Significant improvement has been witnessed for PCE of bulk-heterojunction OPVs through synthesis of new materials and investigation of optimization conditions.^[25,26] However, the performance of OPVs in terms of PCE and stability still falls behind other types of photovoltaic devices due to limitations for further improvement. Narrow absorption windows, high recombination, and low charge carrier mobilities of organic semiconductors are disadvantageous for achieving higher PCE than their counterparts.^[27,28] To overcome the issues mentioned above, two promising methods used are introduction of third component as second donor or acceptor and incorporation of guest materials such as nanoparticles and additives in the active layer. The third component helps to regulate the photovoltaic parameters by improving photocurrent because of their wider absorption spectrum.^[29,30] Properly selected third component based on energy levels establishes another way to reduce energy loss by providing a good match with donor and acceptor energy levels for sufficient electron–hole separation.^[31]

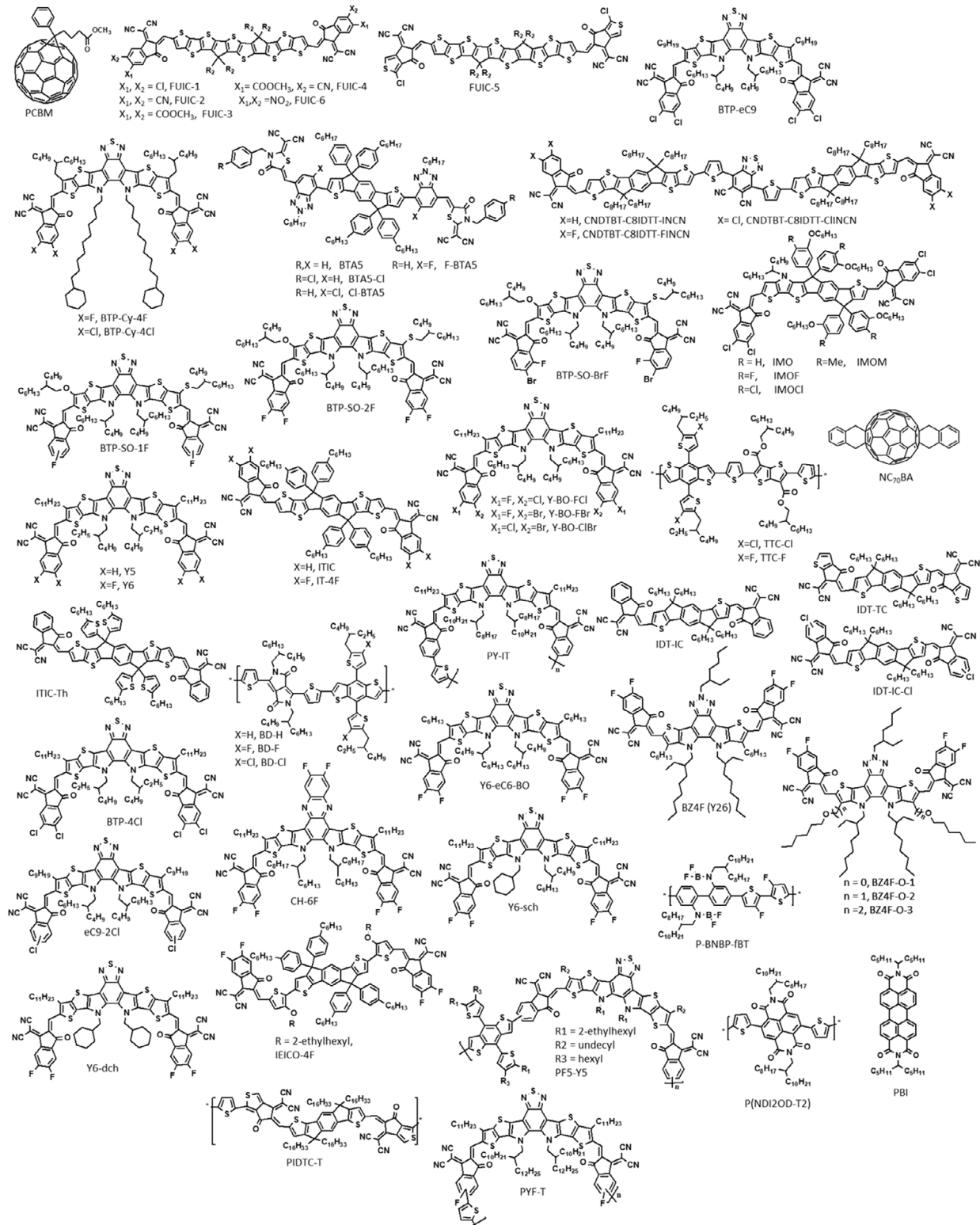
Huang et al.^[32] developed new star-shaped unfused ring-based acceptor materials without and with fluorine-substituent in peripheral group or phenyl core as third components into PM6:Y6 bulk-heterojunction OPVs. The study of structure–property–performance dependence revealed that synthesized acceptors exhibited complementary to Y6 and PM6 in most

aspects important for ternary OPVs such as balanced structure and light absorption, isotropic charge transfer, energy-level cascades of novel star-shaped unfused ring-based acceptor materials with PM6 and Y6. Fluorine-free based third component ternary OPV delivered champion performance with PCE of 16.57% due to enhanced photon harvesting, reduced charge recombination, mediated frontier molecular orbital levels, and improved charge transport. Meng et al.^[29] designed and synthesized novel asymmetric silicon–oxygen bridged third component with blue-shifted absorption spectra, larger dipole moments, and raised LUMO energy levels than symmetric silicon–oxygen-bridged third component. Their ternary OPVs exhibited increased storage stability than binary devices and outstanding PCE of 18.77%, benefiting from simultaneous improved FF of 78.37%, J_{SC} of 26.72 mA cm^{-2} , and V_{OC} of 0.896 V. The outstanding performance of novel asymmetric silicon–oxygen bridged as a third component for this ternary OPV is mainly attributed to enhanced crystallinity, good miscibility with acceptor material, good alignment of energy levels, and complementary absorption. Incorporation of metallic nanoparticles in photoactive layer improves light absorption in the longer wavelength range by possessing surface plasmon resonance effect.^[33,34] This effect increases the concentration of electron–hole pair formation by increasing the optical path in the photoactive layer. Du et al.^[35] incorporated polyelectrolyte polystyrene sulfonate (PSS)-coated plasmonic gold nanorods (GNRs@PSS) into enhance photons absorption and generation of charges via back scattering and near-field plasmonic. GNRs successfully improved photons absorption and increased generation of charges. Negatively charged PPS shell on the surface of GNRs ensured uniform dispersion of GNRs@PSS in the photoactive layer and improved the hole transportation to the electrode. After incorporation of GNRs@PSS in the photoactive layer, the PCE (10.11%) increased by approximately 20% relative to the control OPV (8.47%).

During optimization of PCE in OPVs, the photovoltaic parameters must be carefully studied. The morphology of the active layer film is an important factor altering the performance of OPVs, from light absorption to charge transportation. In the active layer with desired morphology, the donor and acceptor materials are well mixed with good phase separation. However, the actual active layer morphology has defects restricting the performance of OPVs. Many methods such as development of new materials, thermal annealing, and additives have been studied and used to improve active layer morphology.^[36,37] These methods modify the active layer morphology in such a way that the performance of the OPVs improves. Optimization conditions are required after modification of active layer. In this review, we are confident that the discussed OPVs processes and factors affecting the performance of OPVs could give valuable information relevant to help with improving the performance of OPVs. The methods recently used to improve OPVs processes and stability are discussed in this review. Optimization of factors affecting the performance of OPVs such as active layer thickness, solvent and additives, molecular weight of donor/acceptor materials, and annealing temperature are discussed with hope to understand how they change OPVs performance as well as finding their optimal conditions.



Scheme 1. Molecular structure of donor organic molecules.

**Scheme 2.** Molecular structure of acceptor organic molecules.

2. Photovoltaic Processes

The working principle of OPVs is one of the most debated and researched issue. The devices use organic donor and organic acceptor materials, which are sandwiched between transparent and metal electrodes. Transparent electrode allows the light strike active layer of the device. The most used material for transparent electrode is indium tin oxide (ITO) or fluoride tin oxide (FTO) which are supported on a glass substrate.^[38,39] For the metal electrode, metals such as aluminum (Al), gold (Au), and silver (Ag) are mostly used as opaque electrodes.^[40] In OPVs, the acceptor material can be mixed with or deposited onto the donor material to form an active layer. In the active layer, several processes are taking place and are discussed in the following sections. **Schemes 1** and **2** show the molecular structures of donor and acceptor organic molecules used for studies reviewed in this report, respectively.

2.1. Light Absorption

This process is the first one that takes place in the organic active layer. The light travels through the transparent electrode to the active layer. After striking the active layer, light gets absorbed leading to the production of electron–hole pairs. Due to high bandgap of organic materials, utilization of visible–near-infrared region (NIR) of solar spectrum is a problem. The schematic of this process is shown in **Figure 1A**. The metal electrode reflects light that was not absorbed by the donor material in the active layer. There are several ways that are reported to improve light

absorption within OPVs such as light trapping capabilities, increasing the range of absorption spectrum, and adjusting the light absorption ability.^[41]

Ahmed et al.^[42] introduced different concentration of silver-doped magnesium (Ag:Mg) bimetallic nanoparticles in the P3HT:PCBM active layer to improve light absorption (shown in Figure 1B). The UV–vis absorption spectrum of the active layer showed an increase in absorption over the wavelength range from 350 to 900 nm for Ag:Mg bimetallic nanoparticles concentration of 1.5% (see Figure 1C). The improved absorption enhanced the J_{SC} from 11.18 to 14.12 mA cm⁻², leading to an increase in PCE. **Table 1** shows the effect of metallic nanoparticles incorporation on OPVs performance. After the incorporation of metallic nanoparticles, J_{SC} is the parameter, which increased significantly. Therefore, the increase in PCE is due to the increase in J_{SC} because of improved light absorption in the active layer by presence of metallic nanoparticles.

Deng et al.^[43] synthesized nonfullerene acceptors, BTP-Cy-4F and BTP-Cy-4Cl, with absorption coefficient of 1.30×10^5 and 1.34×10^5 M⁻¹ cm⁻¹, respectively. They have absorption spectrum reaching wavelength up to 870 nm (see Figure 1D). When BTP-Cy-4F and BTP-Cy-4Cl individually mixed with D18 donor material, PCE reach 18.52 and 16.50%, respectively. Afterward, a higher PCE of 19.36% was reached by introducing BTP-eC9 as an acceptor material in a BTP-Cy-4F:D18 device. The introduction of BTP-eC9 broadens the absorption spectrum further to 950 nm, resulting in higher J_{SC} of 25.20 mA cm⁻². Alarfaji et al.^[44] reported a series of new fused-ring nonfullerene acceptors having thieno[2,3-b]thiophene-based donor as a core substituted at the end-capped units by synthesized

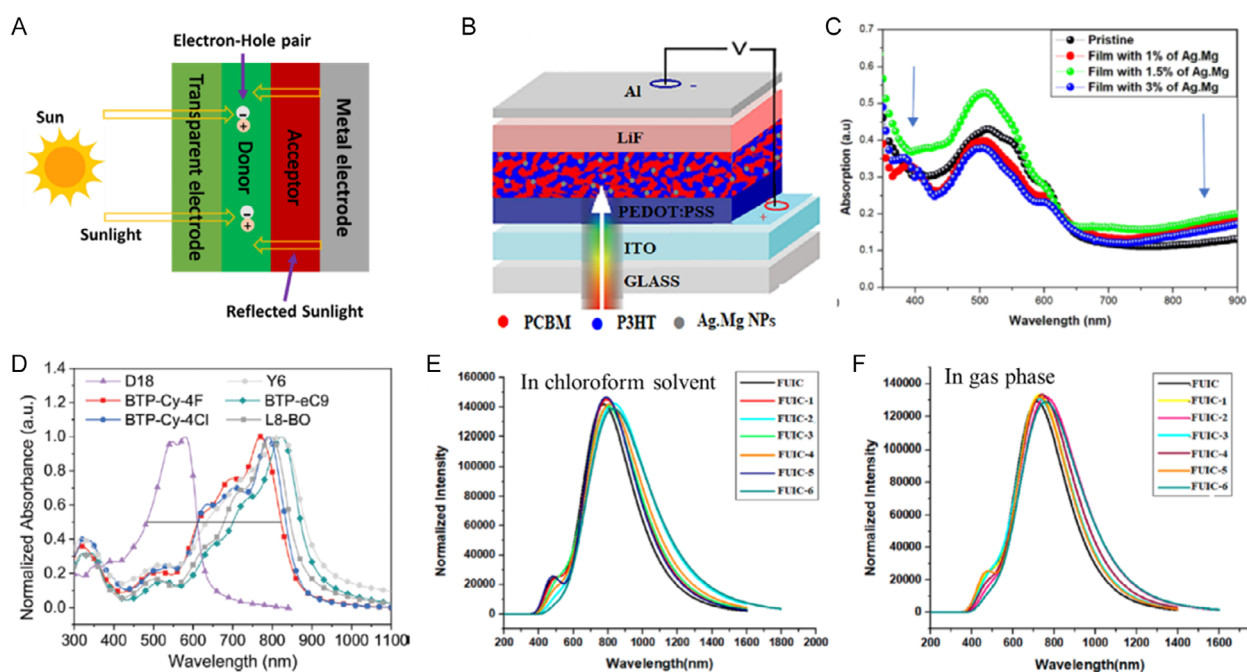


Figure 1. A) Schematic diagram of light absorption process in OPVs cell. B) The architecture for Ag:Mg bimetallic nanoparticles incorporated in P3HT:PCBM device. Reproduced with permission.^[42] Copyright 2023, John Wiley & Sons—Books. C) UV–vis absorption spectra obtained from polymers thin films containing different concentrations of Ag:Mg bimetallic nanoparticles. Reproduced with permission.^[42] Copyright 2023, John Wiley & Sons—Books. D) Normalized UV–vis–NIR absorption spectra of neat films of the relative materials. Reproduced with permission.^[43] Copyright 2023, John Wiley & Sons—Books. UV–vis absorption spectra E) in CF solvent F) in gas phase. Reproduced with permission.^[44] Copyright 2023, American Chemical Society.

Table 1. Effect of nanoparticles incorporation on the performance of OPVs.

Active layer ^{a)}	PCE [%]	J_{SC} [mA cm ⁻²]	FF	V_{OC} [V]	Absorption changes after incorporation of metallic nanoparticles	References
P3HT:PCBM	2.01	8.91	0.43	0.55	Increased absorbance and red-shifted spectra	[91]
P3HT:PCBM: 1 wt% Ag:NiO _x	5.13	19.63	0.47	0.55		
P3HT:PCBM: 3 wt% Ag:NiO _x	4.11	16.09	0.46	0.55		
P3HT:PCBM	3.28	7.83	0.70	0.59	Introduced absorption above P3HT:PCBM absorption edge	[92]
P3HT:PCBM: SiO ₂ @Ag@SiO ₂	7.61	16.31	0.77	0.60	P3HT:PCBM absorption edge	
PIDTT-DFBT:PC ₇₁ BM	7.54	12.66	0.62	0.96	Increased absorbance and red-shifted spectra	[93]
PIDTT-DFBT:PC ₇₁ BM:Ag@TiO ₂	7.56	13.24	0.60	0.95		
PIDTT-DFBT:PC ₇₁ BM:Ag@TiO ₂ @Pa	9.03	14.13	0.65	0.98		
P3HT:PCBM	2.56	11.27	0.42	0.54	Introduced absorption above P3HT:PCBM absorption edge and red-shifted spectra	[94]
P3HT:PCBM: 1 wt% Ni:Zn	4.78	16.71	0.50	0.58		
P3HT:PCBM: 3 wt% Ni:Zn	3.36	13.86	0.44	0.56		
P3HT:PCBM	2.30	9.37	0.50	0.54	Increased absorbance and red-shifted spectra	[95]
P3HT:PCBM: 1 wt% K ₂ S:Ag	5.12	15.80	0.57	0.57		
P3HT:PCBM: 3 wt% K ₂ S:Ag	3.27	11.20	0.53	0.55		
P3HT:PCBM: 5 wt% K ₂ S:Ag	3.20	10.30	0.58	0.54		
P3HT:PCBM	3.06	9.93	0.56	0.55	Increased absorbance and red-shifted spectra	[33]
P3HT:PCBM: 1 wt% Ag:Ag ₂ O	3.23	10.51	0.59	0.54		
P3HT:PCBM: 3 wt% Ag:Ag ₂ O	5.20	16.62	0.59	0.53		
P3HT:PCBM: 5 wt% Ag:Ag ₂ O	3.66	12.24	0.56	0.53		

Abbreviations: ^{a)}P3HT, poly(3-hexylthiophene). PCBM, [6,6]-phenyl-C₆₁-butyric acid methyl ester. Ag:NiO_x, silver:nickel oxide. SiO₂@Ag@SiO₂, silica@silver@silica. PIDTT-DFBT, poly-(indacenodithieno[3,2-b]thiophenedifluorobenzothiadiazole). Ag@TiO₂, silica@titania. Ag@TiO₂@Pa, silica@titania@benzoic-acid-fullerene. Ni:Zn, nickel:zinc. K₂S:Ag, potassium sulfide:silver. Ag:Ag₂O, silver:silver-oxide.

fused-ring-type organic chromophores (F10IC) functionalized with different groups. UV-vis studies were performed and revealed that these nonfullerene acceptors absorb light from visible region to NIR in chloroform (CF) solvent (see Figure 1E) and gas phase (see Figure 1F). The two nitro (NO₂) end-capped nonfullerene acceptor (FUIC-6) has the highest maximum absorption wavelength value because of the extended conjugation and highest electron-withdrawing capacity. Their study reported that FUIC-6 possesses excellent photovoltaic properties such as V_{OC} of 1.10 V, bandgap of 1.88 eV, electron reorganization energy of 0.00431856 eV, and hole reorganization energy of 0.00806781 eV. Their findings suggest that the designed structure of FUIC-6 is the most efficient acceptor used in the study as electron- and hole-transporting material for OPVs with excellent photovoltaic features and can be employed in the next most efficient OPV devices. These findings indicate that the incorporation of metallic nanoparticles in the active layer and modification of nonfullerene acceptors with electron-withdrawing groups improve the light absorption features within the device and increases the number of electron–hole pair generated. Table 2 shows the studies performed to improve the absorption of the active layer by modifying the acceptor material. The studies revealed that the acceptor material substituted with high electron-withdrawing group has narrow optical bandgap with improved J_{SC} and PCE.

2.2. Exciton Diffusion

After generation of electron–hole pair, they diffuse to donor/acceptor interface. A schematic of this process is shown in Figure 2A. The electron–hole pairs with large diffusion length can travel to donor/acceptor interface and thus contribute to PCE if the coulombic-bound electron–hole pairs are not dissociated within their lifetime.^[45] One of the main issues is to enhance the diffusion length of electron–hole pair, because longer diffusion lengths for electron–hole pairs in OPVs are expected to allow electron–hole separation and reduced charge recombination. The electron–hole pair diffusion length (L_D) is a physical quantity known by Equation (1):

$$L_D = (D\tau)^{\frac{1}{2}} \quad (1)$$

where D is diffusion coefficient and τ is an electron–hole pairs lifetime. The lifetime of most conjugated polymers is typically less than 1 ns, limiting the diffusion lengths to 10 nm.^[46] As a result, limited part of the electron–hole pair generated will diffuse to donor/acceptor interface in bilayer OPVs. Therefore, bulk heterojunction OPVs are introduced to harvest more electron–hole pairs at donor/acceptor interface. Electron–hole pairs can easily reach the interface once the domain size of acceptor and donor materials is less than the diffusion length. Therefore,

Table 2. Effect of acceptor substituents on the performance of OPVs.

Active layer ^{a)}		Acceptor ^{b)} substituent	Acceptor bandgap [eV]	PCE [%]	J_{SC} [mA cm^{-2}]	FF	V_{OC} [V]	References
Donor	Acceptor							
PBDB-T	CNDTBT-C8IDTT-INCN	INCN	1.39	7.54	14.18	0.62	0.86	[96]
PBDB-T	CNDTBT-C8IDTT-FINCN	FINCN	1.37	12.06	20.77	0.70	0.83	
PBDB-T	CNDTBT-C8IDTT-ClINCN	ClINCN	1.36	11.32	21.67	0.67	0.78	
PTQ10	BTAs	—	1.76	4.49	5.69	0.61	1.29	[97]
PTQ10	BTAs-Cl	Cl	1.77	8.78	10.29	0.69	1.23	
PTQ10	Cl-BTAs	Cl	1.74	11.00	13.13	0.70	1.19	
PM6	IMO	—	1.40	14.56	22.95	0.71	0.89	[98]
PM6	IMOF	F	1.39	14.71	24.01	0.78	0.79	
PM6	IMOCl	Cl	1.43	13.21	23.35	0.74	0.77	
PM6	IMOM	Me	1.42	13.71	23.00	0.69	0.87	
PM6	BTP-SO-BrF	Br, F	1.46	15.50	22.61	0.73	0.94	[99]
PM6	BTP-SO-1F	F	1.47	16.20	23.17	0.74	0.94	
PM6	BTP-SO-2F	F, F	1.45	17.60	24.54	0.79	0.91	
D18	BTf	F (direct coupled)	1.31	16.83	27.19	0.72	0.86	[100]
D18	BTfM	F (indirect coupled)	1.33	17.10	26.72	0.73	0.87	
PM6	Y-BO-FCI	F, Cl	1.33	17.52	26.45	0.78	0.85	[101]
PM6	Y-BO-FBr	F, Br	1.32	16.47	25.83	0.75	0.85	
PM6	Y-BO-ClBr	Cl, Br	1.33	13.61	22.09	0.72	0.86	
TTC-F	BTAs	—	—	9.81	12.21	0.65	1.22	[102]
TTC-F	F-BTAs	F	—	10.57	13.93	0.67	1.13	
TTC-Cl	BTAs	—	—	8.65	10.66	0.64	1.25	
TTC-Cl	F-BTAs	F	—	10.98	13.38	0.70	1.17	

Abbreviations: ^{a)}PBDB-T, Poly[[4,8-bis[5-(2-ethylhexyl)-2-thienyl]benzo[1,2-b:4,5-b']dithiophene-2,6-diy]-2,5-thiophenediy][5,7-bis(2-ethylhexyl)-4,8-dioxo-4H,8H-benzo[1,2-c:4,5-c']dithiophene-1,3-diyl]] polymer. CNDTBT-C8IDTT-INCN, 4,7-bis(9-(2-Methylene-((3-(1,1-dicyanomethylene)-6,7-dihydro-indanone))-5,5,11,11-tetrakis(octyl)-dithieno[2,3-d:2',3'-d']-s-indaceno[1,2-b:5,6-b']dithiophene)- 5,6-dicyano-2,1,3-benzothiadiazole. PTQ10, poly[(thiophene)-alt-(6,7-difluoro-2-(2-hexyldecyloxy)quinoxaline)]. CNDTBT-C8IDTT-FINCN, 4,7-bis(9-(2-Methylene-((3-(1,1-dicyanomethylene)-6,7-difluoro-indanone))-5,5,11,11-tetrakis(octyl)-dithieno[2,3-d:2',3'-d']-s-indaceno[1,2-b:5,6-b']dithiophene)- 5,6-dicyano-2,1,3-benzothiadiazole. CNDTBT-C8IDTT-ClINCN, 4,7-bis(9-(2-Methylene-((3-(1,1-dicyanomethylene)-6,7-dichloro-indanone))-5,5,11,11-tetrakis(octyl)-dithieno[2,3-d:2',3'-d']-s-indaceno[1,2-b:5,6-b']dithiophene)- 5,6-dicyano-2,1,3-benzothiadiazole. BTA, benzotriazole. IMO, indeno(dithieno[3,2-b:2',3'-d]pyrrol) substituted hexyloxyphenyl. PM6, poly[[4,8-bis[5-(2-ethylhexyl)-4-fluoro-2-thienyl]benzo[1,2-b:4,5-b']dithiophene-2,6-diy]-2,5-thiophenediy][5,7-bis(2-ethylhexyl)-4,8-dioxo-4H,8H-benzo[1,2-c:4,5-c']dithiophene-1,3-diyl]-2,5-thiophenediy]. BTP-SO-BrF, dithienothiopheno[3,2-b]-pyrrolobenzothiadiazole substituted (5-bromo-4-fluoro-3-oxo-2,3-dihydro-1H-inden-1-ylidene)malononitrile. BTP-SO-1F, dithienothiopheno[3,2-b]-pyrrolobenzothiadiazol substituted 2-(6-fluoro-3-oxo-2,3-dihydro-1H-inden-1-ylidene)malononitrile. BTP-SO-2F, dithienothiopheno[3,2-b]-pyrrolobenzothiadiazole substituted 2-(5,6-difluoro-3-oxo-2,3-dihydro-1H-inden-1-ylidene)malononitrile. BTF, direct fluorinated benzothiazole. BTFM, indirect fluorinated benzothiazole. Y-BO, fused benzothiadiazole. TTC, carboxylate-substituted thienothiophene; ^{b)}INCN, 2-(3-oxo-2,3-dihydro-1H-inden-1-ylidene)malononitrile. FINCN, 2-(5,6-difluoro-3-oxo-2,3-dihydro-1H-inden-1-ylidene)malononitrile. Cl, chlorine. F, fluorine. Me, methyl. Br, Bromine.

understanding the exciton diffusion dynamics can help to further optimize active layer thickness and develop new donor materials with high electron–hole transportation properties to improve OPVs performance.^[46]

Studies revealed that exciton diffusion length can be increased by use of donor or acceptor materials which contain heavy atoms that permit intersystem crossing and by doping active layer with triple sensitizers.^[47] Yang et al.^[48] investigated electron donor materials of 2-(5"-tert-butyl-[2,2':5',2"-terthiophen]-5-yl)benzo[d]thiazole (tTBz) ligand, platinum (II) complex (tTBzPt), octahedral homoleptic iridium (III) complex (tTBz3Ir), and octahedral heteroleptic tTBzIr complex for OPVs. The molecular geometries of these donor materials were investigated using density

functional theory (see Figure 2B). The tTBz showed a linear molecular skeleton, tTBzPt exhibited planar geometry and Ir(III) complexes showed octahedral geometry. The spatially twisted geometries of tTBzIr and tTBz3Ir inhibit triplet–triplet annihilation for improved triplet features and decrease in intermolecular interactions. The photoluminescence spectra of tTBz-based complexes are depicted in Figure 2C and corresponding transient photoluminescence decay curves are shown in Figure 2D. Monomodal profile was observed for tTBz and tTBzPt with PL lifetimes measured at 0.51 and 0.25 ns, respectively, indicative of singlet features. The tTBzIr and tTBz3Ir complexes showed multimodal profile with the intense emission peaks at shorter wavelength due to singlet-centered emission

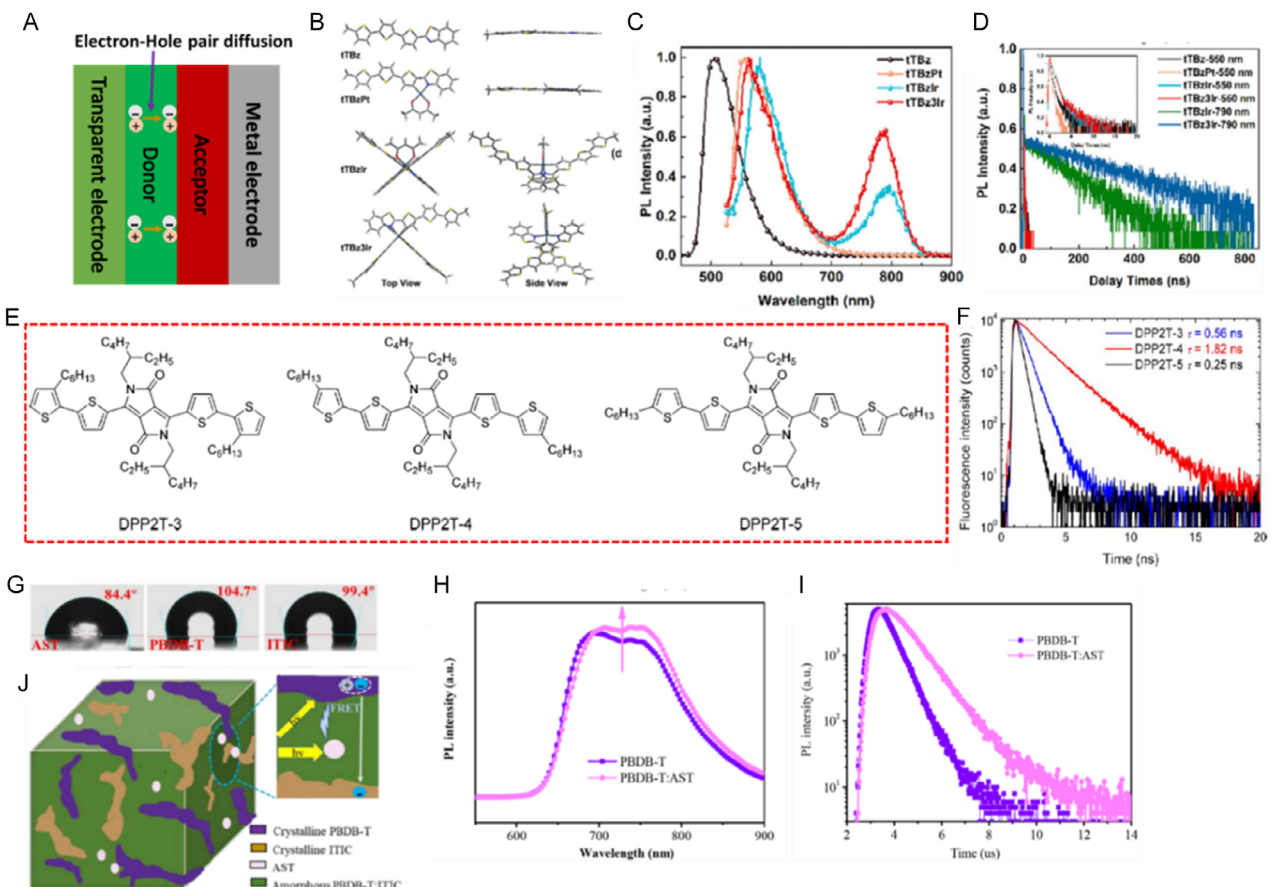


Figure 2. A) Schematic diagram of exciton diffusion process in OPVs cell. B) Simulated structural geometries of the compounds. C) Normalized photoluminescence spectra of synthesized compounds and D) corresponding transient photoluminescence decay curves recorded at 550 and 790 nm. Reproduced with permission.^[48] Copyright 2023, Royal Society of Chemistry. E) Molecular structure of DPP2T-3, DPP2T-4, and DPP2T-5. F) Time-resolved fluorescence intensity recorded at 840 nm for thin films of DPP2T-3, DPP2T-4, and DPP2T-5. Reproduced with permission.^[49] Copyright 2014, American Chemical Society. G) Contact angle studies of AST, PBDB-T, and ITIC films. H) Photoluminescence spectra of the PBDB-T and PBDB-T: 0.1 wt% AST. I) Time-resolved photoluminescence spectra of the PBDB-T and PBDB-T: 0.1 wt% AST. J) Graphic illustration of possible molecular distribution in AST containing OPVs. Reproduced with permission.^[50] Copyright 2023, Elsevier.

which can be observed by their <1 ns photoluminescence lifetime. The lower intense peaks at longer wavelength were assigned to triplet-dominated phosphorescence according to increased lifetime (116 ns for tTBzIr and 276 ns for tTBz3Ir). The longer lifetime and increased phosphorescent intensity achieved in tTBz3Ir are indicative of longer electron–hole diffusion length than tTBzIr. Therefore, these finding are beneficial to facilitate sufficient electron–hole dissociation and reduced recombination which might improve OPVs performance.

Gevaerts et al.^[49] studied the effect of hexyl side chains position on the optical properties of isomers based on diketopyrrolopyrrole and bithiophene (DPP2T) with their structures, as shown in Figure 2E. The fluorescence studies revealed that the maximum peak was found for DPP2T-4 at longer wavelength and the lifetime is much longer than DPP2T-3 and DPP2T-5 (see Figure 2F). Therefore, electron–hole diffusion length is prolonged in DPP2T-4. This study indicated that the position of substituents does have an influence on the diffusion length of the compound. Huang et al.^[50] studied addition of environmentally

friendly astaxanthin (AST) into the active layer comprised of PBDB-T and ITIC. The possible molecular distribution within the active layer is shown in Figure 2J. Contact angle studies indicated that AST has stronger hydrophilicity and higher surface energy than PBDB-T and ITIC (Figure 2G). Therefore, the molecules of AST will be distributed in the blend phases between crystalline PBDB-T and ITIC. The reduced distance between PBDB-T and AST enhances the Förster resonant energy transfer (FRET) efficiency as observed in Figure 2H by increase in intensity. Transfer of photons energy absorbed by AST to PBDB-T prolongs the lifetime of electron–hole pair (see Figure 2I). The electron–hole pair lifetime for PBDB-T and PBDB-T:AST were measured to be 0.67 and 1.11 ns, respectively.

2.3. Exciton Dissociation/Separation

During exciton separation, the coulombically bound electron–hole pair separates into free charges (an electron and a hole). This separation takes place at donor/acceptor interface which

facilitates electron transfer from donor material to acceptor material by construction of charge transfer state leaving a hole in the donor material. This process is shown schematically in Figure 3A. The lowest unoccupied molecular orbitals (LUMO) of the donor material must be higher than that of acceptor material for successful electron–hole separation. The difference in LUMO energy levels of donor and acceptor materials must be around 0.2–0.3 eV and higher than the electron–hole pair binding energy for sufficient electron–hole separation.^[51] At the charge transfer state, electron and hole that are next to each other have a chance to recombine and drop to the ground state. If recombination takes place, there will be a loss in terms of charge separation process which is one of the reasons why OPVs have low efficiency.^[52,53]

The studies showed that the nature of donor and acceptor materials influences the LUMO energy levels. Park et al.^[54] reported synthesis of halogenated derivatives of BD-H for use as donor materials (see Figure 3B). Halogenated derivatives of BD-H (BD-Cl and BD-F) showed higher V_{OC} , FF, and PCE due to their deeper LUMO energy levels (see Figure 3C). The electron-withdrawing ability of halogens cause a downshift on the LUMO energy levels resulting in a decrease in LUMO offset (ΔE_{LUMO}). Therefore, higher electron–hole dissociation (η_{diss}) achieved in BD-Cl:Y6 (PCE = 5.62% and η_{diss} = 84.50%) and BD-F:Y6 (PCE = 5.20% and η_{diss} = 77.70%) devices compared to BD-H:Y6 (PCE = 4.93% and η_{diss} = 72.00%) device is one of the causes on the improvement of OPVs performance (see Figure 3D). Yoon et al.^[28] synthesized donor materials based on cyclopentadithiophene core, as shown in Figure 3E. The LUMO energy levels of PL1 and PL2 were estimated from the difference in HOMO energy level determined by cyclic voltammetry and the energy bandgap. Figure 3F shows the energy levels diagram of PL1 and PL2 compared to the LUMO energy levels of acceptors (Y6 and PC₆₁BM). PL1 has deeper LUMO energy level than PL2. The LUMO offsets are smaller for PL1:PC₆₁BM

(0.09 eV) and PL2:PC₆₁BM (0.12 eV) composites than for PL1:Y6 (0.35 eV) and PL2:Y6 (0.38 eV) with PL1:PC₆₁BM having the smallest LUMO offset value because of deeper energy levels of PL1. To investigate their OPVs properties, PC₆₁BM was used as a bridge for charges because of the wider LUMO offset values of PL1:Y6 and PL2:Y6 composites. This method successfully improved overall performance from PCE = 6.55% for PL1:Y6 to PCE = 7.54% for PL1:Y6:PC₆₁BM and from PCE = 10.12% for PL2:Y6 to 11.62% with PL2:Y6:PC₆₁BM by reducing ΔE_{LUMO} using bridging material which is indicative of electron–hole dissociation increase (see Figure 3G).

The introduction of the third material in the active layer of bulk heterojunction OPVs to form a ternary device has been widely investigated. This type of device offers an opportunity to improve electron–hole dissociation for achieving high FF and PCE. The studies showing the comparison of the binary and ternary OPVs are summarized in Table 3. The presence of bridging material in the ternary OPVs divides the ΔE_{LUMO} into two compared to binary OPVs: ΔE_{LUMO} between the donor material and the bridging material ($\Delta E_{LUMO(Ter\ 1)}$) and ΔE_{LUMO} between the bridging material and acceptor material ($\Delta E_{LUMO(Ter\ 2)}$). The values of $\Delta E_{LUMO(Ter\ 1)}$ and $\Delta E_{LUMO(Ter\ 2)}$ are lower than the ΔE_{LUMO} of binary OPVs. Therefore, the introduction of bridging material increases η_{diss} by reducing the ΔE_{LUMO} leading to a decrease in electron–hole recombination, consequently improving the PCE, FF, and V_{OC} in ternary OPVs.

2.4. Charge Transportation

After separation of exciton at donor/acceptor interface, electrons travel through the acceptor material to the active layer/cathode (metal electrode) interface while holes are transported to the active layer/anode (ITO electrode) interface via the donor material (see Figure 4A). The charge transport is also affected by recombination and the interaction of charges with atoms or other

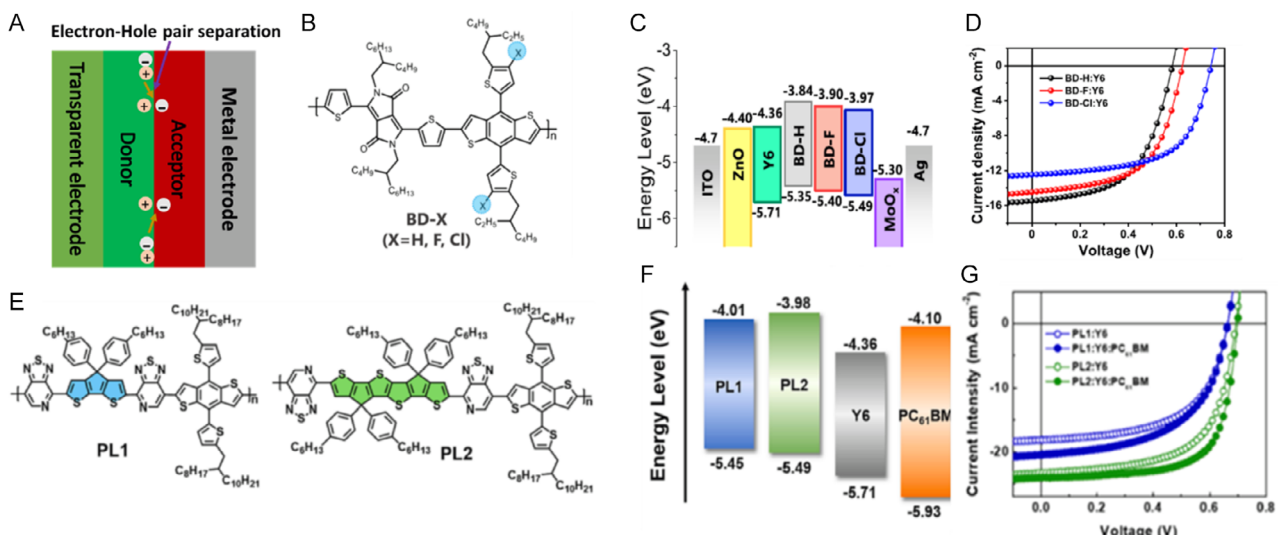


Figure 3. A) Schematic diagram of exciton separation process in OPVs. B) Structures of BD-X (X = H, F, Cl). C) Energy level diagram and schematic illustration of the OPV device structure. D) J–V curves of the BD-H:Y6, BD-F:Y6, and BD-Cl OPVs. Reproduced with permission.^[54] Copyright 2023, Elsevier. E) Chemical structures and F) energy level diagrams of PL1 and P2. G) J–V curves of PL1- and PL2-based OPVs. Reproduced with permission.^[28] Copyright 2023, Elsevier.

Table 3. Effect of the third component in an active layer on the ΔE_{LUMO} and OPV performance.

Active layer ^{a)}	$\Delta E_{\text{LUMO(Bin)}}^{\text{b)}}$ [eV]	$\Delta E_{\text{LUMO(Ter 1)}}^{\text{c)}}$ [eV]	$\Delta E_{\text{LUMO(Ter 2)}}^{\text{d)}}$ [eV]	$\eta_{\text{diss}}^{\text{e)}}$ [%]	PCE [%]	J_{SC} [mA cm ⁻²]	FF	V_{OC} [V]	References
D18-Cl:N3	0.76	—	—	98.20	16.54	26.74	0.72	0.86	[103]
D18-Cl:BTR-Cl:N3	—	0.36	0.40	99.10	17.92	27.92	0.75	0.85	
PM6:PY-IT	0.29	—	—	90.90	15.39	22.80	0.72	0.94	[104]
PM6:PC ₇₁ BM	0.15	—	—	90.40	8.40	13.95	0.62	0.98	
PM6:PY-IT:PC ₇₁ BM	—	0.15	0.14	95.50	16.11	23.68	0.73	0.94	
P:IDT-TC	0.23	—	—	96.30	14.26	19.88	0.69	1.04	[105]
P:IDT-IC-Cl	0.38	—	—	95.40	13.34	22.64	0.67	0.88	
P:IDT-TC:IDT-IC-Cl	—	0.23	0.15	98.40	16.44	23.98	0.71	0.96	
PM7:Y6	0.48	—	—	97.20	14.44	24.55	0.69	0.85	[106]
PM7:Y6: NC ₇₀ BA	—	0.15	0.33	97.60	15.70	25.35	0.71	0.87	
PM6:IT4F	0.47	—	—	86.10	13.11	20.62	0.74	0.85	[107]
PM6:IT4F:PC ₇₁ BM	—	0.33	0.14	89.73	13.73	21.48	0.75	0.85	
D18:CH-6 F	0.85	—	—	96.30	16.86	25.54	0.73	0.90	[108]
D18:FSBTSeHR:CH-6F	—	0.62	0.23	97.90	18.55	26.91	0.76	0.91	
D18:FSBTSeEHR:CH-6F	—	0.59	0.26	97.20	18.02	26.41	0.75	0.91	
B2:Y6	0.91	—	—	93.60	8.73	16.38	0.65	0.84	[109]
B3:Y6	0.81	—	—	95.20	9.26	19.43	0.67	0.72	
B2:B3:Y6	—	0.10	0.81	97.80	12.88	22.62	0.73	0.78	
PM6:Y6	0.64	—	—	96.50	15.80	25.50	0.74	0.85	[110]
PM6: 0.1 PBDTDTzT:Y6	—	0.11	0.53	99.50	17.00	26.30	0.75	0.86	
PM6: 0.2 PBDTDTzT:Y6	—	—	—	97.90	15.70	25.60	0.71	0.87	
PM6: 0.3 PBDTDTzT:Y6	—	—	—	98.30	15.50	25.00	0.71	0.87	

Abbreviations: ^{a)}D18-Cl, Poly[(2,6-(4,8-bis(5-(2-ethylhexyl-3-chloro)thiophen-2-yl)-benzo[1,2-b:4,5-b']dithiophene))-alt-5,5'-(5,8-bis(4-(2-butyloctyl)thiophen-2-yl)dithieno[3',2':3,4;2'',3'':5,6]benzo[1,2-c][1,2,5]thiadiazole)]. N3, 2,2'-(2Z,2'Z)-((12,13-bis(3-ethylheptyl)-3,9-diundecyl-12,13-dihydro-[1,2,5]thiadiazolo[3,4-e]thieno[2'',3'':4';5']thieno[2',3':4,5]pyrrolo[3,2-g]thieno[2',3':4,5]thieno[3,2-b]indole-2,10-diyl)bis(methanlylidene))bis(5,6-difluoro-3-oxo-2,3-dihydro-1H-indene-2,1-diylidene)dimalononitrile. BTR, 5,5'- [[4,8-bis[5-(2-ethylhexyl)-4-hexyl-2-thienyl]benzo[1,2-b:4,5-b']dithiophene-2,6-diyl]bis[(3',3''-dihexyl[2,2':5',2''-terthiophene-5'',5-diyl)methylidyne]]bis[3-hexyl-2-thioxo-4-thiazolidinone]. IDT-TC, 2,2'-(5Z,5'-5,5'-(4,4,9,9-Tetrahexyl-4,9-dihydro-s-indaceno[1,2-b:5,6-b']dithiophene2,7-diyl)bis(methanlylidene))bis(6-oxo-5,6-dihydro4H-cyclopenta[b]thiophene-5,4-diylidene)) dimalononitrile. IDT-IC-Cl, 2,2'-(2Z,2'Z)-((4,4,9-tris(4-hexylphenyl)-4,9-dihydro-s-indaceno[1,2-b:5,6-b']dithiophene-2,7-diyl)bis(4-((2-ethylhexyl)oxy)thiophene-5,2-diyl)bis(methanlylidene))bis(5,6-dichloro-3-oxo-2,3-dihydro-1H-indene-2,1-diylidene))dimalononitrile. PM7, Poly[(2,6-(4,8-bis(5-(2-ethylhexyl-3-chloro)thiophen-2-yl)-benzo[1,2-b:4,5-b']dithiophene))-alt-(5,5-(1',3'-di-2-thienyl-5',7'-bis(2-ethylhexyl)benzo[1',2':c:4',5'-c']dithiophene-4,8-dione)]. Y6, 2,2'-(2Z,2'Z)-((12,13-bis(2-ethylhexyl)-3,9-diundecyl-12,13-dihydro-[1,2,5]thiadiazolo[3,4-e]thieno[2'',3'':4',5']thieno[3,2-b]indole-2,10-diyl)bis(methanlylidene))bis(5,6-difluoro-3-oxo-2,3-dihydro-1H-indene-2,1-diylidene))dimalononitrile. NC₇₀BA, [6,6]-Phenyl-C71-butyric acid methyl ester. IT4F, 3,9-bis(2-methylene-((3-(1,1-dicyanomethylene)-6,7-difluoro)-indanone))-5,5,11,11-tetrakis(4-hexylphenyl)-dithieno[2,3-d:2',3'-d'-s-indaceno[1,2-b:5,6-b']dithiophene. PBTDTDzT, 5-(4,8-bis(4,5-diocetylthiophen-2-yl)-6-methylbenzo[1,2-b:4,5-b']dithiophen-2-yl)-2-(5-(5-methylthiazol-2-yl)thiophen-2-yl)thiazole. BD-H, Poly[2,6'-4,8-di(5-ethylhexylthienyl)benzo[1,2-b:3,4-b]dithiophene-alt-5-diethyl-octyl-3,6-bis(5-bromo-5-ethylthienyl)pyrrole[3,4-c]pyrrole-1,4-dione]; ^{b)} $\Delta E_{\text{LUMO(Bin)}}$, LUMO offset of binary OPVs; ^{c)} $\Delta E_{\text{LUMO(Ter 1)}}$, LUMO offset between the donor and bridging material; ^{d)} $\Delta E_{\text{LUMO(Ter 2)}}$, LUMO offset between the bridging and donor acceptor material; ^{e)} η_{diss} , exciton dissociation.

charges that may decrease the rate they travel leading to a decrease in PCE of OPVs. To improve the charge transportation in OPVs, tailoring the morphology of the active layer is very important because charge transport is dependent on it.^[55] Modifying the chemical structure of either acceptor or donor material proved to be effective in adjusting the morphology of the active layer. Modification of donor and acceptor material with side chains attached to the central core has the ability to adjust the interactions between molecules, improve solubility, and adjust the molecular packing during film formation.^[36] The presence of smaller side chains may induce stronger molecular interactions, causing an increase in phase separation of the active layer film. The molecular backbone with large volume of side

chains could provide good processability by improving solubility but may affect the molecular packing behavior and reduce the charge transportation. Therefore, it is very important to balance the solubility and molecular packing to achieve better charge transportation.

Wang et al.^[56] presented synthesis of hybrid side chains comprised of cyclopentane, cyclohexane, and cycloheptane introduced to the tail of hexyl side chain to prepare new D18-based donor materials. The relative degree of crystallinity reduced after modification of D18 while maintaining compact molecular packing with terminal cyclic chain provides disturbance on aggregation (see Figure 4B). These findings are beneficial for effective electron–hole separation and balanced charge transport. These

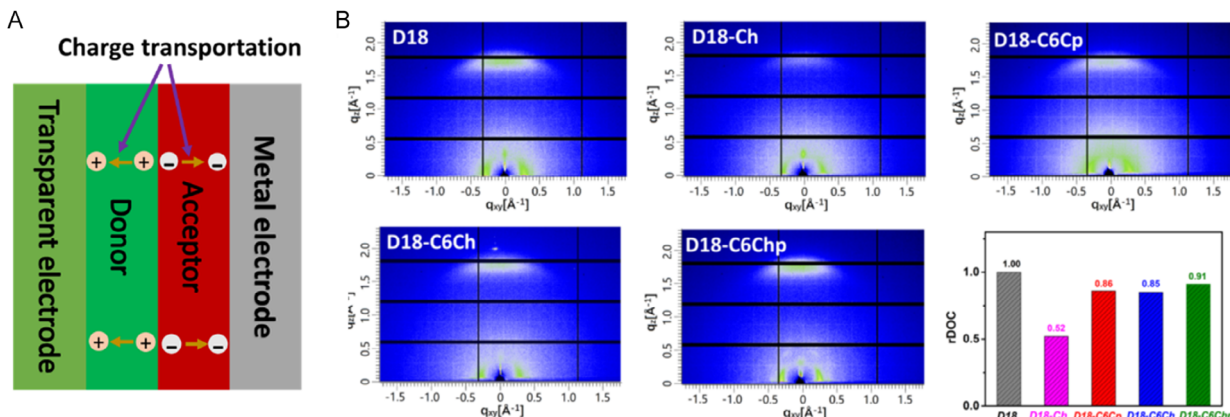


Figure 4. A) Schematic diagram of charge transportation process in OPVs cell. B) 2D grazing-incidence wide-angle X-ray scattering diffraction patterns of D18 and D18-R neat films. Reproduced with permission.^[56] Copyright 2022, Elsevier.

hybrid side chains influenced self-assembling characteristics and easing the interpenetrating network of active layer contributing to sufficient charge transport. The champion performance was achieved for hexyl-cyclohexyl modified-D18-based OPV (PCE = 18.2%) with highest electron mobility (μ_e) of $4.91 \times 10^{-4} \text{ cm}^2 \text{ V}^{-1} \text{ s}^{-1}$ and hole mobility (μ_h) of $4.85 \times 10^{-4} \text{ cm}^2 \text{ V}^{-1} \text{ s}^{-1}$. The work showed effective hybrid hexyl-based side chains engineering with better crystallinity improves charge transport and OPVs performance. Some of the work done on the tuning of charge transportation using alkyl side chains are recorded in Table 4. The studies show that there is no specific trend between the side chain size and the charge transportation. Different side chains on either acceptor or donor material having different central cores tailor the morphology differently; therefore, improving the charge transport in OPVs to different extent.

2.5. Charge Collection

To generate current, the holes must be collected at the anode while electrons must be collected at the cathode. The current is flow of electrons through the connecting conductor on the anode and cathode of the OPVs, which draws current off for external use, as shown in Figure 5A. The cell voltage results from cell build-in electricity together while the cell current defines the cell power produced. The current flow is directed by employing electrodes with dissimilar work functions. The anode is elected to have a high work function while the cathode is elected to have a low work function. Electrons will travel through the low work function cathode while holes will travel through high work function anode. Mostly, modified layers such as PEDOT:PSS are inserted between active layer and anode as hole transport layer while metal oxides such as zinc oxide and titanium oxide are inserted between cathode and organic active layer as electron transport layer. These modified layers permit only specific carrier charge type to pass through to the matching electrode.^[57–59]

Hou et al.^[58] used PEDOT:PSS hole transport layer (HTL) and they further incorporated different concentrations of titanium carbide ($\text{Ti}_3\text{C}_2\text{T}_x$) MXene into it. They obtained the charge conductivity study of PEDOT: PSS/ $\text{Ti}_3\text{C}_2\text{T}_x$ composite by four-point probe measurements. The incorporation of $\text{Ti}_3\text{C}_2\text{T}_x$ nanoflakes

in PEDOT:PSS significantly increases the conductivity of the composites (see Figure 5B). In relation to hole transport, space charge-limited current was used to confirm the enhancement of μ_h after the incorporation of $\text{Ti}_3\text{C}_2\text{T}_x$ nanoflakes with an optimal concentration of 0.15%. The μ_h increased to $7.09 \times 10^{-4} \text{ cm}^2 \text{ V}^{-1} \text{ s}^{-1}$ after $\text{Ti}_3\text{C}_2\text{T}_x$ nanoflakes incorporation from $4.37 \times 10^{-4} \text{ cm}^2 \text{ V}^{-1} \text{ s}^{-1}$ for pure PEDOT:PSS-based OPV (see Figure 5C). PEDOT:PSS conductivity model was proposed after the incorporation of $\text{Ti}_3\text{C}_2\text{T}_x$ nanoflakes (see Figure 5D). The functional groups such as $-\text{O}-$, $-\text{OH}$, and $-\text{F}$ present in $\text{Ti}_3\text{C}_2\text{T}_x$ nanoflakes electrostatically interact with the sulfonic acid of PSS. These reduce the coulombic interaction between PEDOT and PSS leading to a change in PEDOT conformation to linear or expanded-coil structure increasing interchain charge transport. However, incorporating high concentration of $\text{Ti}_3\text{C}_2\text{T}_x$ nanoflakes reduces the charge transport by aggregation of $\text{Ti}_3\text{C}_2\text{T}_x$ due to weakened phase separation. PEDOT:PSS/ $\text{Ti}_3\text{C}_2\text{T}_x$ -based OPVs demonstrated excellent stability compared to PEDOT:PSS-based OPV because of alleviated corrosion of PEDOT:PSS on the active layer and ITO substrate (see Figure 5E). Wang et al.^[60] incorporated alkali metal salts (lithium acetate (LiAc) or cesium acetate (CsAc)) into ZnO electron transport layer (ETL). The incorporation of alkali salts significantly increased PCE because their presence improves light trapping and J_{SC} . Photoluminescence was used to investigate the interfacial trap passivation of doped and undoped ZnO thin films (see Figure 5F). The decrease in photoluminescence intensity observed after doping with LiAc and CsAc indicates a decrease in defects of ZnO, resulting in improvement in charge collection and reduced charge recombination. Their study proved that the incorporation of alkali metals into ZnO thin films is beneficial to improve electron collection and transport (see Figure 5G). Compared to undoped ZnO device, μ_e significantly increased for OPVs with doped ZnO, due to enhanced mechanical adhesion between the hydrophilic alkali metal salts of doped ZnO and active layer. Table 5 summarizes some of the work done on the improvement of electron and hole collection layers. Incorporation of adequate concentration of nanoparticles or small organic molecules in electron and hole transport layers improves the charge mobility and conductivity resulting in better performance of OPVs.

Table 4. Side-chain effect on the charge transportation and performance of OPVs.

Active layer ^{a)}	Side chain	μ_e [cm ² v ⁻¹ s ⁻¹]	μ_h [cm ² v ⁻¹ s ⁻¹]	PCE [%]	J_{SC} [mA cm ⁻²]	FF	V _{OC} [V]	References
BBTSM-1:Y6	C ₉ H ₁₉ , C ₈ H ₁₇	2.41×10^{-4}	4.06×10^{-4}	11.80	21.60	0.63	0.87	[111]
BBTSM-2:Y6	C ₁₉ H ₃₅ , C ₆ H ₁₃	0.17×10^{-4}	3.41×10^{-4}	5.70	16.70	0.44	0.78	
PM6-T:Y6	–	1.37×10^{-3}	1.61×10^{-3}	17.11	25.03	0.77	0.85	[112]
PM6-T-C1:Y6	CH ₃	1.21×10^{-3}	1.50×10^{-3}	16.54	24.86	0.75	0.85	
PM6-T-C6:Y6	C ₆ H ₁₃	0.61×10^{-3}	0.91×10^{-3}	16.23	25.11	0.74	0.85	
PM6-T-C12:Y6	C ₁₂ H ₂₅	0.53×10^{-3}	0.83×10^{-3}	15.98	24.89	0.73	0.84	
PM6:Y6	C ₁₁ H ₂₃ , C ₈ H ₁₇	6.15×10^{-5}	7.20×10^{-5}	9.02	18.45	0.63	0.78	[113]
PM6:Y6-eC6-BO	C ₆ H ₁₃ , C ₁₂ H ₂₅	4.54×10^{-4}	4.55×10^{-4}	16.38	25.72	0.76	0.84	
PM6:BZ4F	–	1.90×10^{-5}	1.50×10^{-5}	13.79	22.53	0.72	0.85	[114]
PM6:BZ4F-O-1	OC ₆ H ₁₃	2.40×10^{-5}	2.30×10^{-5}	13.50	19.57	0.76	0.91	
PM6:BZ4F-O-2	OC ₇ H ₁₅	1.90×10^{-5}	2.00×10^{-5}	13.43	21.62	0.75	0.82	
PM6:BZ4F-O-3	OC ₈ H ₁₇	1.90×10^{-5}	2.20×10^{-5}	14.69	23.51	0.74	0.85	
PM6: Y6-sch	C ₆ H ₁₁	4.74×10^{-4}	5.39×10^{-4}	16.01	25.46	0.73	0.86	[115]
PM6: Y6-dch	Two C ₆ H ₁₁	4.01×10^{-4}	5.15×10^{-4}	14.19	22.76	0.74	0.84	
TBCA-C2:IT-4F	C ₂ H ₅	7.65×10^{-5}	1.52×10^{-5}	7.34	13.61	0.59	0.91	[116]
TBCA-C4:IT-4F	C ₄ H ₉	1.12×10^{-4}	1.06×10^{-4}	9.21	15.43	0.64	0.93	
TBCA-C6:IT-4F	C ₆ H ₁₃	8.07×10^{-5}	2.42×10^{-5}	7.91	13.97	0.60	0.94	
TBCA-C8:IT-4F	C ₈ H ₁₇	6.92×10^{-5}	1.38×10^{-5}	7.24	13.52	0.57	0.94	

Abbreviations: ^{a)}IT-4F, 3,9-bis(2-methylene-((3-(1,1-dicyanomethylene)-6,7-difluoro)-indanone))-5,5,11,11-tetrakis(4-hexylphenyl)-dithieno[2,3-d:2',3'-d']-s-indaceno[1,2-b:5,6-b']dithiophene. Y6-eC6-BO, 2,2'-(((Z,Z')-((12,13-bis(2-butyloctyl)-3,9-dihexyl-12,13-dihydro-[1,2,5]thiadiazolo[3,4-e]thieno[2",3":4',5']thieno[2',3':4,5]pyrrolo[3,2-g]thieno[2",3":4,5]thieno[3,2-b]indole-2,10-diyl)bis(methanlylidene))bis(5,6-difluoro-3-oxo-2,3-dihydro-1H-indene-2,1-diylidene))dimalononitrile. BZ4F, 2,2'-(((Z,Z')-((12,13-bis(2-ethylhexyl)-3,9-dihexyl-12,13-dihydro-[1,2,5]thiadiazolo[3,4-e]thieno[2",3":4',5']thieno[2',3':4,5]pyrrolo[3,2-g]thieno[2",3":4,5]thieno[3,2-b]indole-2,10-diyl)bis(methanlylidene))bis(5,6-difluoro-3-oxo-2,3-dihydro-1H-indene-2,1-diylidene))dimalononitrile. BZ4F-O-1, 2,2'-(((Z,Z')-((12,13-bis(2-ethylhexyl)-3,9-dihexyloxy-12,13-dihydro-[1,2,5]thiadiazolo[3,4-e]thieno[2",3":4',5']thieno[3,2-b]indole-2,10-diyl)bis(methanlylidene))bis(5,6-difluoro-3-oxo-2,3-dihydro-1H-indene-2,1-diylidene))dimalononitrile. BZ4F-O-2, 2,2'-(((Z,Z')-((12,13-bis(2-ethylhexyl)-3,9-dihexyloxy-12,13-dihydro-[1,2,5]thiadiazolo[3,4-e]thieno[2",3":4',5']thieno[3,2-b]indole-2,10-diyl)bis(methanlylidene))bis(5,6-difluoro-3-oxo-2,3-dihydro-1H-indene-2,1-diylidene))dimalononitrile. BZ4F-O-2, 2,2'-(((Z,Z')-((12,13-bis(2-ethylhexyl)-3,9-dihexyloxyethyl-12,13-dihydro-[1,2,5]thiadiazolo[3,4-e]thieno[2",3":4',5']thieno[2',3':4,5]pyrrolo[3,2-g]thieno[2",3":4,5]thieno[3,2-b]indole-2,10-diyl)bis(methanlylidene))bis(5,6-difluoro-3-oxo-2,3-dihydro-1H-indene-2,1-diylidene))dimalononitrile. Y6-sch, 2,2'-(((Z,Z')-((12,13-bis(2-ethylhexyl)-3,9-diundecyl-12,13-dihydro-[1,2,5]thiadiazolo[3,4-e]thieno[2",3":4',5']thieno[2',3':4,5]pyrrolo[3,2-g]thieno[2",3":4,5]thieno[3,2-b]indole-2,10-diyl)bis(methanlylidene))bis(5,6-difluoro-3-oxo-2,3-dihydro-1H-indene-2,1-diylidene))dimalononitrile. Y6-dch, 2,2'-(((Z,Z')-((12-(2-butyloctyl)-13-(cyclohexylmethyl)-3,9-diundecyl-12,13-dihydro-[1,2,5]thiadiazolo[3,4-e]thieno[2",3":4',5']thieno[2',3':4,5]pyrrolo[3,2-g]thieno[2",3":4,5]thieno[3,2-b]indole-2,10-diyl)bis(methanlylidene))bis(5,6-difluoro-3-oxo-2,3-dihydro-1H-indene-2,1-diylidene))dimalononitrile. BBTSM-1, 4,8-Bis-(5-(2-ethylhexyl)-thiophen-2-yl)-2,6-dimethyl-berizo[1,2-d;4,5-d']bisthiazole. BBTSM-1, 4,8-Bis-(5-(2-ethylhexyl)-thiophen-2-yl)-2,6-bis(2-cyano-3-(3',3-octyl-[2,2';5',2"]terthiophen-5-yl)-acrylic acid 2-ethyl-hexyl ester)-berizo[1,2-d;4,5-d']bisthiazole. BBTSM-2, 4,8-Bis-(5-(2-hexyldecyl)-thiophen-2-yl)-2,6-bis(2-cyano-3-(3',3-hexyl-[2,2';5',2"]terthiophen-5-yl)-acrylic acid 2-ethyl-hexyl ester)-berizo[1,2-d;4,5-d']bisthiazole. TBCA-C2, 2,6-Bis-[4,8-Bis-(5-(2-ethylhexyl)-thiophen-2-yl)-6-(2-cyano-acrylic acid ethyl acetoxy)-1,7-dithia-s-indacen-2-yl]-4,8-bis-(5-(2-ethylhexyl)-thiophen-2-yl)-1,5-dithia-s-indacene. TBCA-C4, 2,6-Bis-[4,8-Bis-(5-(2-ethylhexyl)-thiophen-2-yl)-6-(2-cyano-acrylic acid butyl acetoxy)-1,7-dithia-s-indacen-2-yl]-4,8-bis-(5-(2-ethylhexyl)-thiophen-2-yl)-1,5-dithia-s-indacene. TBCA-C6, 2,6-Bis-[4,8-Bis-(5-(2-ethylhexyl)-thiophen-2-yl)-6-(2-cyano-acrylic acid hexyl acetoxy)-1,7-dithia-s-indacen-2-yl]-4,8-bis-(5-(2-ethylhexyl)-thiophen-2-yl)-1,5-dithia-s-indacene. TBCA-C8, 2,6-Bis-[4,8-Bis-(5-(2-ethylhexyl)-thiophen-2-yl)-6-(2-cyano-acrylic acid octyl acetoxy)-1,7-dithia-s-indacen-2-yl]-4,8-bis-(5-(2-ethylhexyl)-thiophen-2-yl)-1,5-dithia-s-indacene.

3. Optimization of OPVs Active Layer

3.1. Thickness of the Active Layer

An active layer is inserted between two electrodes that have dissimilar work functions. Investigations revealed that as the active layer thickness is tempered, the performance of the device dramatically changes. As the active layer thickness increases, more light is absorbed resulting in high J_{SC} which is due to the generation of sufficient electron–hole pairs.^[61] Since PCE of OPVs does not depend only on J_{SC} , some parameters are affected as the thickness of the active layer increases. **As the thickness increases, charge carrier transport and collection are**

affected due to an increase in interface defect states and low charge mobility resulting in an increase in charge carrier recombination. This lowers the FF and V_{OC} which are the reason for a dramatical decrease in PCE as the thickness of the active layer increases.^[62]

To overcome these challenges, donor and acceptor materials with high charge mobility, ordered molecular structure, high light absorption abilities, and good morphology need to be developed. Yang et al.^[63] reported the effect of active layer thickness on OPVs performance. They investigated how the increase in active layer thickness from 30 to 200 nm affects the performance of OPVs (see Figure 6A). The best PCEs were achieved for devices with an active layer thickness of \approx 100 nm. Zhang et al.^[64]

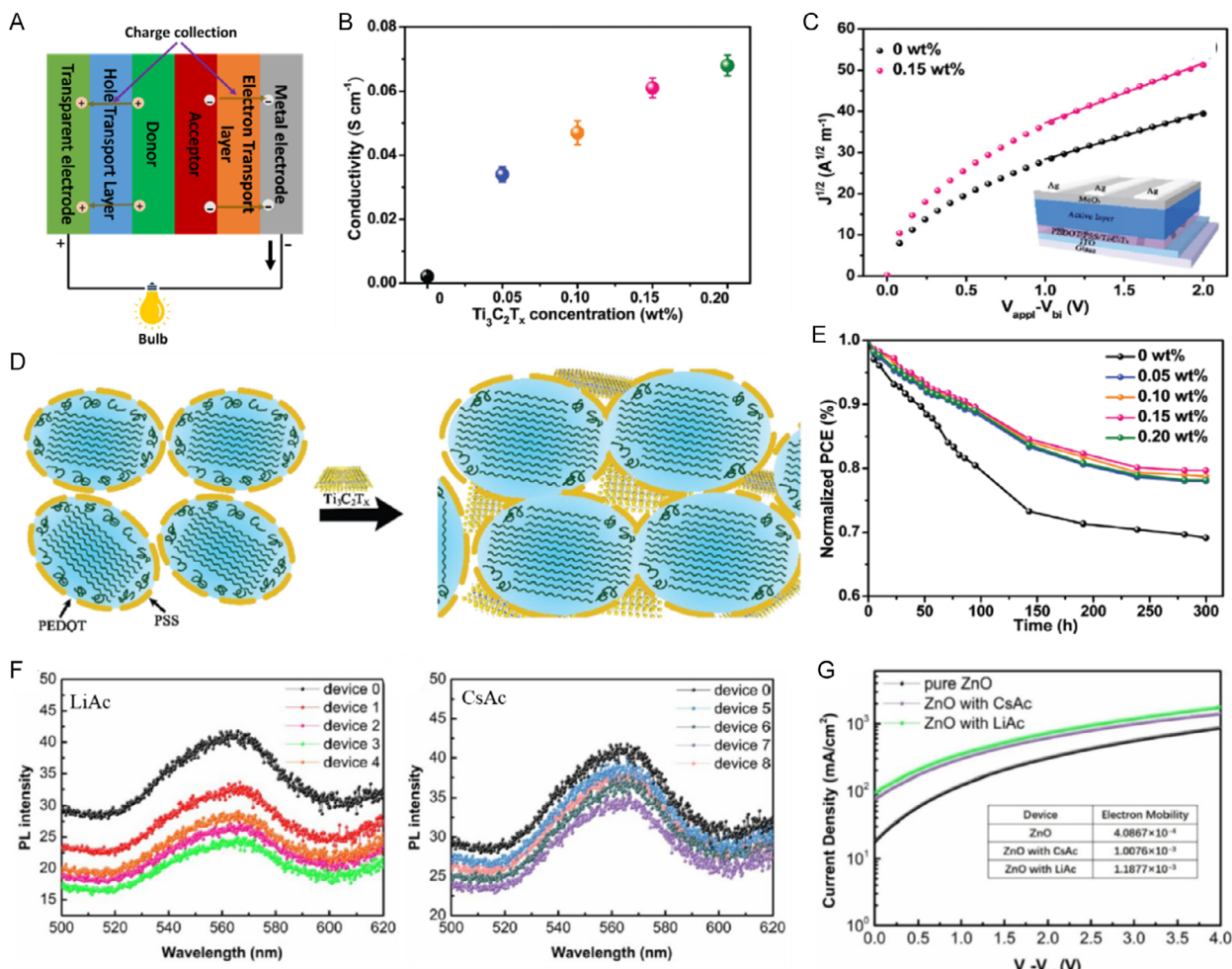


Figure 5. A) Schematic diagram of the charge collection process in OPVs cell. B) Conductivity studies of glass-coated PEDOT:PSS and PEDOT:PSS/Ti₃C₂T_x films. C) J-V curves of the hole-only devices in the dark. D) Graphic demonstration of structural modifications before and after incorporation of Ti₃C₂T_x in PEDOT:PSS. E) Stability test of OPVs with different concentrations of Ti₃C₂T_x in PEDOT:PSS in a N₂ glove box. Reproduced with permission.^[58] Copyright 2020, The Royal Society of Chemistry. F) Photoluminescence spectra of ZnO with different concentrations of LiAc and CsAc. G) J-V curves of electron-only device. Reproduced with permission.^[60] Copyright 2019, Elsevier.

investigated the thickness of PM6:IT-4F active layer prepared by blade-coating at various temperatures and spin coating having different thicknesses from 79 to 515 nm. The best PCE was obtained at thicknesses of 103, 132, 134, and 141 nm for spin-coated OPV, and blade-coated at 30, 50, and 70 °C, respectively (see Figure 6B). The thickness of PM6:IT-4F active layer, PCE, and J_{SC} increases until optimal thickness and then decreases, while FF and V_{OC} both decrease (see Figure 6B–E). Table 6 shows recent studies based on how active layer thickness influences the OPVs performance. The high performance of OPVs was achieved when the active layer thickness was \approx 100 nm. OPVs with active layer thickness of \approx 100 nm are more efficient because of their balanced μ_e and μ_h values with their ratio close to 1. When the active layer thickness increases, series resistance (R_{series}) and the shunt resistance (R_{shunt}) decrease. These indicate that as the active layer thickness increases, charge recombination dominates due to an increase in charge diffusion length.

3.2. Solvent and Additives

During the preparation of the active layer of OPVs, it is important to choose a good solvent to study the properties of the active layer that can help in predicting what is affecting the performance of the device. There are several factors that must be taken into consideration when choosing the solvent such as ability to dissolve donor and acceptor materials to allow proper mixing, not form a complex with either donor or acceptor material, and have not a very high boiling point.^[65] Mostly used solvents for preparation of the active layer are chlorinated for example chlorobenzene (CB), dichlorobenzene (DCB), o-dichlorobenzene (o-DCB), dichloromethane (DCM), and CF. It was revealed that solvent caused dramatic change in the performance of the device. Solvents affect the morphology of the active layer, which affects the OPVs properties and crystallinity that determines the charge carrier mobility. The use of solvents with low drying speed (high boiling point) like CB improves the FF and J_{SC} by increasing the

Table 5. Modification of electron and hole transport layers by incorporating a third component in OPV applications.

ETL ^a /HTL ^b	Dopant ^a)	μ_e [cm ² v ⁻¹ s ⁻¹]	μ_h [cm ² v ⁻¹ s ⁻¹]	Conductivity [S cm ⁻¹]	PCE [%]	J_{SC} [mA cm ⁻²]	FF	V_{OC} [V]	References
PEDOT:PSS ^h	0.00% Nb ₂ C	—	7.34×10^{-5}	3.23×10^{-4}	17.17	26.26	0.78	0.84	[117]
	0.10% Nb ₂ C	—	2.22×10^{-4}	8.13×10^{-4}	18.30	27.21	0.80	0.84	
	0.00% Ag NWs	—	—	8.28×10^{-2}	12.96	19.74	0.75	0.88	[118]
	3.00% Ag NWs	—	—	9.12×10^{-2}	13.14	19.91	0.75	0.88	
	5.00% Ag NWs	—	—	9.54×10^{-2}	13.53	20.76	0.75	0.87	
	8.00% Ag NWs	—	—	9.78×10^{-2}	12.65	20.32	0.72	0.87	
	0.00% α -In ₂ Se ₃	—	2.06×10^{-4}	2.21×10^{-3}	10.21	15.78	0.70	0.90	[119]
	0.15% α -In ₂ Se ₃	—	3.44×10^{-4}	4.63×10^{-3}	11.22	17.03	0.71	0.91	
	0.00% WS ₂ NS	—	2.00×10^{-4}	—	14.35	24.08	0.72	0.83	[120]
	1.00% WS ₂ NS	—	2.35×10^{-4}	—	15.31	25.20	0.73	0.83	
	3.00% WS ₂ NS	—	3.32×10^{-4}	—	15.69	25.55	0.74	0.83	
	5.00% WS ₂ NS	—	2.52×10^{-4}	—	15.52	25.32	0.74	0.84	
	0.00 mg mL ⁻¹ g-C ₃ N ₄	—	3.23×10^{-4}	9.00×10^{-2}	15.29	25.63	0.71	0.84	[121]
	0.40 mg mL ⁻¹ g-C ₃ N ₄	—	6.34×10^{-4}	18.00×10^{-2}	16.38	26.71	0.73	0.84	
ZnO ^e	0.00 mg mL ⁻¹ DA	—	2.74×10^{-4}	9.04×10^{-4}	16.01	25.19	0.76	0.84	[122]
	1.00 mg mL ⁻¹ DA	—	4.27×10^{-4}	3.78×10^{-3}	16.55	25.52	0.77	0.84	
	0.00% CA	1.25×10^{-4}	—	1.53×10^{-4}	10.15	16.91	0.68	0.88	[123]
	0.10% FA	4.18×10^{-4}	—	4.72×10^{-4}	11.75	18.24	0.71	0.91	
	0.10% DMCA	3.42×10^{-4}	—	3.95×10^{-4}	11.25	17.92	0.70	0.90	
	0.00% Ti ₃ C ₂ T _x	2.51×10^{-4}	—	3.66×10^{-4}	11.15	17.85	0.69	0.90	
	0.05% Ti ₃ C ₂ T _x	8.61×10^{-5}	—	1.31×10^{-4}	10.68	16.82	0.68	0.93	[124]
	0.00% PDA-Ti ₃ C ₂ T _x	4.51×10^{-4}	—	2.46×10^{-4}	12.31	18.63	0.70	0.93	
	0.09% PDA-Ti ₃ C ₂ T _x	2.69×10^{-4}	—	1.20×10^{-4}	10.45	16.53	0.67	0.93	[125]
	0.00 mg mL ⁻¹ Glycine	5.54×10^{-4}	—	2.52×10^{-4}	12.19	18.14	0.71	0.94	
	0.75 mg mL ⁻¹ Glycine	1.63×10^{-4}	—	—	12.90	21.30	0.72	0.84	[126]
	0.00% RGO	4.20×10^{-4}	—	—	14.00	22.00	0.75	0.85	
	50.00% RGO	—	—	1.78×10^{-4}	3.00	8.73	0.57	0.60	[127]
	50.00% RGO & 0.10% PEIE	—	—	2.85×10^{-4}	3.42	9.28	0.61	0.60	
	0.10% PEIE	—	—	3.76×10^{-4}	3.83	9.82	0.64	0.61	

Abbreviations: ^aNb₂C, Niobium carbide. Ag NWs, Silver nanowires. α -In₂Se₃, α -phase indium selenide. WS₂ NS, Tungsten disulfide nanosheets. g-C₃N₄, Graphitic carbon nitride. DA, Dopamine. CA, Caffeic acid. FA, ferulic acid. DMCA, 3, 4-dimethoxy cinnamic acid. Ti₃C₂T_x, Titanium carbide. RGO, Reduced graphene oxide. PEIE, Polyethyleneimine ethoxylated; ^bPEDOT:PSS, poly(3,4-ethylenedioxythiophene):polystyrene sulfonate.

crystallinity of the active layer.^[66,67] The use of additives such as 1,8-diiodooctane and mixing of solvents are methods employed to improve the solute affinity.^[68] Additives also play a crucial role in charge carrier mobility, crystallinity, morphology, and PCE depending on their interaction with the donor or acceptor materials.^[69]

Zhou et al.^[70] investigated the effect of solvent on the performance of PM7:IT-4F nonfullerene OPVs using o-xylene (OX) as host solvent and DCM as a guest solvent to control the active layer morphology. Figure 7A shows that the addition of DCM into OX causes an increase in the light absorption intensity with PM7:IT-4F film prepared using 0.90 OX: 0.10 DCM exhibits the highest absorbance. A quenching effect was observed when comparing the emission intensity of PM7 and PM7:IT-4F films prepared in

OX (see Figure 7B). For the PM7:IT-4F film prepared in 0.90 OX: 0.10 DCM, the intensity of the emission peak was suppressed further, which is indicative of efficient electron-hole dissociation and charge carrier transport. Atomic force microscopy (AFM) topography and phase images confirmed that the addition of DCM, the root-mean-square (rms) roughness increases from 2.67 to 4.94 nm (see Figure 8). This increase in rms roughness indicates crystallization improvement and enlarged phase domain providing a good channel for charge carrier transport. Yang et al.^[1] studied the addition of methoxy methyl phenyl sulfide (MMPS) additive in PTB7-Th:PC₇₁BM-based OPV. They found that MMPS controlled the aggregation and blending of acceptor and donor materials to form a good bicontinuous interpenetrating network, which enhanced charge transportation and

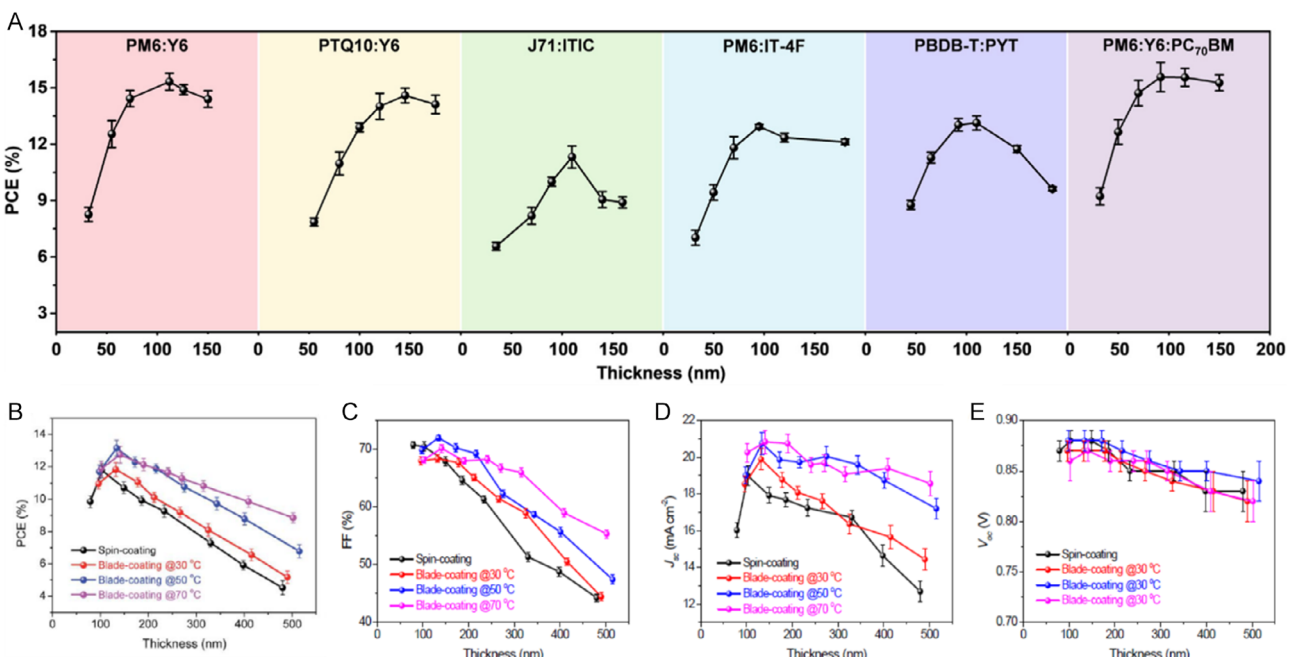


Figure 6. A) OPVs performance with different active layer thicknesses measured at one sun. Reproduced with permission.^[63] Copyright 2021, Elsevier. B) PCE, C) FF, D) J_{SC} , and E) V_{OC} values versus the thickness of the active layer for PM6:IT-4F devices. Reproduced with permission.^[64] Copyright 2019, The Royal Society of Chemistry.

reduced charge recombination. Subsequently, the performance of PTB7-Th:PC₇₀BM-based OPV improved from 4.80% without MMPS to 9.24% with MMPS. The effect of solvents and additives on the performance of OPVs is given and compared in Table 7. The studies recorded in Table 7 revealed that after the addition of additives in the active layer, the performance of OPVs improves. Solvents and additives help in tuning the morphology of the active layer resulting in the increase in charge mobility and more balanced charge transportation to respective electrodes.

3.3. Molecular Weight of Donor and Acceptor Materials

The main idea in OPVs field is to understand the relation between the structural properties that rule the performance of the material. The changes in the chemical structure of a donor material have been shown to affect properties such as light absorption, charge carrier transport, morphology, and electronic agreement with acceptor materials.^[71–73] However, the inclusion of substituents like alkyl chains and fluorine turns to further improve these properties. Nevertheless, they turn to affect the conduction properties and decrease the crystallinity of the active layer materials (donor and acceptor).^[74,75] To overcome the OPVs performance limitations, optimization and development of new organic donor and acceptor materials are required. This is why understanding the relationship between the active layer materials and the OPVs performance is necessary. Therefore, the effect of the molecular weight of donor and acceptor materials on OPVs performance has been investigated.

Zhang et al.^[76] investigated molecular weight effect on the active layer morphology and OPVs performance. Their study revealed that as the molecular weight increases, J_{SC} and FF

increase progressively, while V_{OC} displays negligible change. As shown in Figure 9A, lower molecular weight *P*-BNBP-fBT blend with DR3TBDTC film, large discontinuous DR3TBDTC crystallites, and long *P*-BNBP-fBT fibers were observed. For mid-molecular weight of *P*-BNBP-fBT (Figure 9B), the crystalline domains of DR3TBDTC shrink and fibers of *P*-BNBP-fBT are not so obvious. For higher molecular weight *P*-BNBP-fBT blend (Figure 9C), DR3TBDTC domains are distributed homogeneously throughout the film and large number of narrow *P*-BNBP-fBT fibers were observed. The decrease in DR3TBDTC crystalline domains was attributed to restrict motion, which limits the crystal growth. The decrease in the size of *P*-BNBP-fBT fibers was due to the slow diffusion of high molecular weight polymer and an increase in nucleation density. Photoluminescence spectra comparison of pristine and blend films are depicted in Figure 9D. The donor/acceptor quenching efficiency of 64.10/87.80, 75.60/91.90, and 80.90/94.70% was determined for lower, mid, and higher molecular weight *P*-BNBP-fBT, respectively. The highest photoluminescence quenching efficiency achieved in high molecular weight *P*-BNBP-fBT supports the small-size phase separation revealed by transmission electron microscopy (TEM) studies. Kang et al.^[77] investigated the effect of PPDT2FBT molecular weight on structural, morphological, and photovoltaic properties. As shown in Figure 10a–c, larger aggregates in the PPDT2FBT: P(NDI2OD-T2) blends were observed for PPDT2FBT with the lowest molecular weight and finer domains were observed in the blend with the highest molecular weight PPDT2FBT. Additionally, surface roughness and domain size of the blends decreased as the molecular weight of PPDT2FBT increased, demonstrating suppression of microscopic phase separation in

Table 6. OPVs performance with different active layer thickness.

Active layer ^{a)}	Thickness [nm]	μ_e [$\text{cm}^2 \text{V}^{-1} \text{s}^{-1}$]	μ_h [$\text{cm}^2 \text{V}^{-1} \text{s}^{-1}$]	μ_h/μ_e	PCE [%]	J_{SC} [mA cm^{-2}]	FF	V_{OC} [V]	R_{series} [Ωcm^2]	R_{shunt} [Ωcm^2]	References
PBDB-T-2Cl:BTP-4F	100	1.31×10^{-6}	2.30×10^{-6}	1.76	15.7	25.80	0.70	0.85	—	—	[128]
	200	1.92×10^{-6}	8.50×10^{-6}	4.43	13.00	24.90	0.61	0.82	—	—	
	300	4.51×10^{-6}	1.39×10^{-5}	3.08	12.20	27.60	0.54	0.82	—	—	
PM6:Y6	60	—	—	—	14.14	22.34	0.74	0.86	2.30	2026	[129]
	80	—	—	—	15.29	24.19	0.74	0.86	2.40	1975	
	100	—	—	—	15.83	25.39	0.73	0.86	2.60	1823	
	120	—	—	—	15.34	25.71	0.70	0.85	3.00	1573	
	140	—	—	—	15.10	25.87	0.69	0.85	3.30	1361	
	160	—	—	—	14.35	25.32	0.67	0.85	3.50	1196	
	180	—	—	—	13.58	24.81	0.65	0.84	4.20	1060	
PBDB-T-2Cl:BTP-4F	100	—	—	—	14.62	21.73	0.77	0.88	3.03	—	[130]
	200	—	—	—	14.17	22.19	0.73	0.87	3.78	—	
	300	—	—	—	13.29	22.42	0.69	0.86	4.63	—	
	380	—	—	—	11.81	21.81	0.64	0.85	5.63	—	
PM6:IT-4F	79	—	—	—	11.78	18.99	0.71	0.88	—	—	[64]
	103	—	—	—	10.72	17.92	0.68	0.88	—	—	
	149	—	—	—	9.94	17.68	0.65	0.87	—	—	
	186	—	—	—	9.27	17.24	0.61	0.85	—	—	
	233	—	—	—	7.30	16.72	0.51	0.85	—	—	
	330	—	—	—	5.62	14.63	0.49	0.83	—	—	
	398	—	—	—	4.52	12.68	0.44	0.83	—	—	
PTB7:PC ₇₀ BM	100	—	—	—	5.29	11.55	0.62	0.74	11.71	1070	[131]
	200	—	—	—	3.75	11.00	0.44	0.71	18.70	224	
PM6:Y6	100	2.30×10^{-3}	2.75×10^{-3}	1.20	15.89	25.13	0.74	0.85	—	—	[132]
	300	2.10×10^{-4}	5.00×10^{-4}	2.38	12.94	26.41	0.60	0.82	—	—	

Abbreviations: ^{a)}PBDB-T-2Cl, Poly[(2,6-(4,8-bis(5-(2-ethylhexyl-3-chloro)thiophen-2-yl)-benzo[1,2-b:4,5-b']dithiophene))-alt-(5,5-(1',3'-di-2-thienyl-5',7'-bis(2-ethylhexyl)benzo[1',2'-c:4',5'-c']dithiophene-4,8-dione))]. BTP-4F, 2,2'-(2Z,2'Z)-(12,13-bis(2-ethylhexyl)-3,9-diundecyl-12,13-dihydro-[1,2,5]thiadiazolo[3,4-e]thieno[2",3":4",5"]thieno[2',3':4,5]pyrrolo[3,2-g]thieno[2',3':4,5]thieno[3,2-b]indole-2,10-diyl)bis(methanonylidene))bis(5,6-difluoro-3-oxo-2,3-dihydro-1H-indene-2,1-diylidene)dimalononitrile. PTB7, Poly [(4,8-bis(2-ethylhexyl)oxy)benzo[1,2-b:4,5-b']dithiophene-2,6-diyl][3-fluoro-2-(2-ethylhexyl)carbonyl]thieno[3,4-b]thiophenediyl]. BP-4F, benzo [1,2- b:4,5- b 'di (cyclopenta [2,1-b:3,4- b ']dithiophene) with 4- (5,6-difluoro-3-oxo-2,3-dihydro-1H-inden-1-ylidene)-malanonitrile.

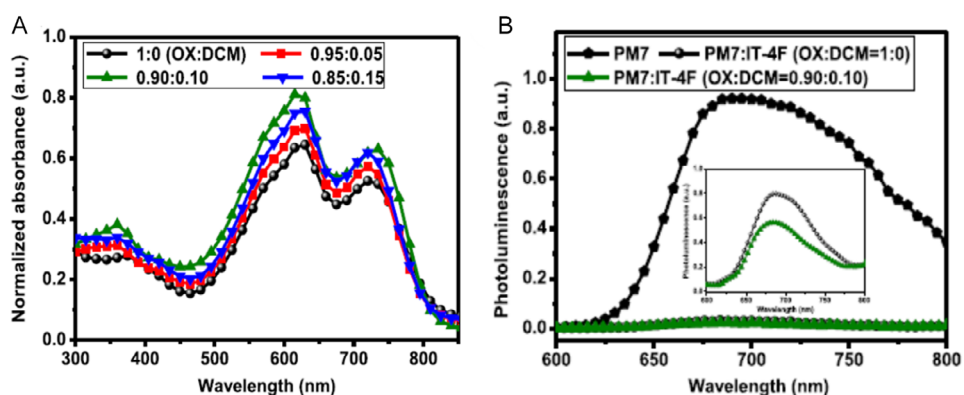


Figure 7. A) Normalized UV–vis absorption and B) photoluminescence spectra of the active layer films prepared with single and binary solvents. Reproduced with permission.^[70] Copyright 2021, American Chemical Society.

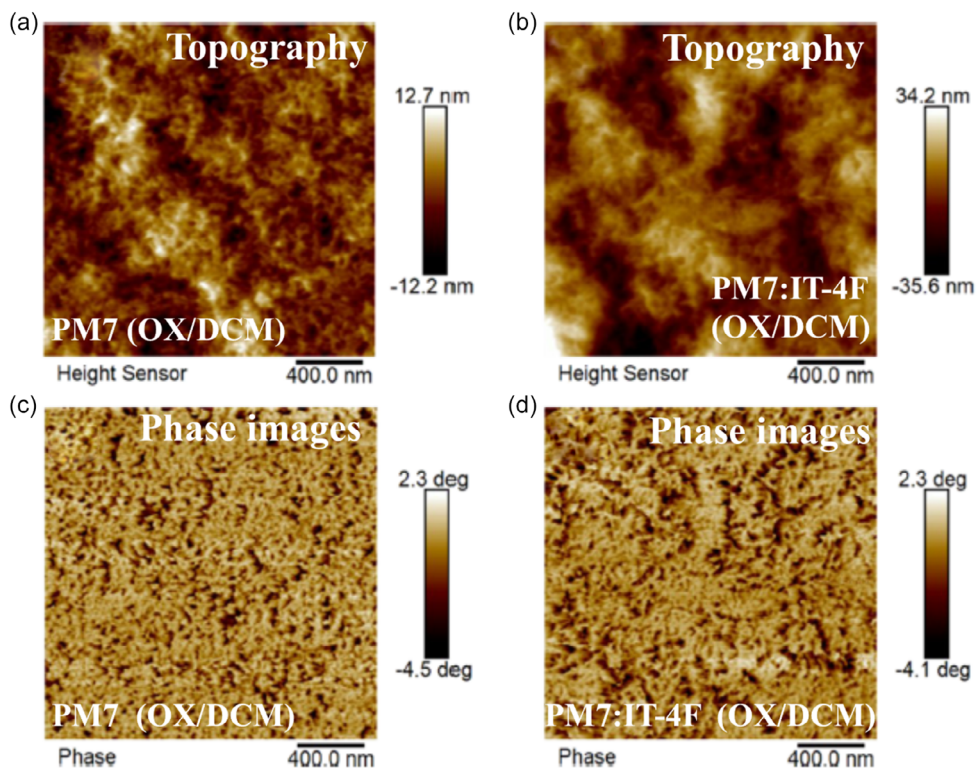


Figure 8. AFM topography and corresponding phase images of a,c) PM7 film and b,d) PM7:IT-4F film prepared in a mixture of OX/DCM solvents. Reproduced with permission.^[70] Copyright 2021, American Chemical Society.

the highest molecular weight PPDT2FBT containing blend. Therefore, OPV based on highest molecular weight PPDT2FBT as a donor material showed the highest electron and hole mobilities, leading to maximum PCE. **Table 8** shows the studies done to understand how molecular weight of the donor and acceptor materials affect OPVs performance. The best performance of OPVs was achieved for donor and acceptor with higher molecular weight. As the molecular weight increases, PCE, J_{SC} , and FF increase. But, at too high molecular weight, the overall OPVs performance decreases. Electron and hole mobilities increase as the molecular weight increases. There is no specific trend for optical bandgap and LUMO offset as the molecular weight of either donor or acceptor increases.

3.4. Annealing Temperature

The performance of the OPVs can also be affected by fabrication conditions such as annealing time and annealing temperature. **Annealing conditions alter with active layer morphology, which consequently affects the PCE.** Morphology of the active layer should be tuned in such a way that it allows efficient separation and transportation of charges. The way of tuning the morphology is by annealing where it facilitates the aggregations that depend on the annealing conditions of the active layer.^[78,79] Therefore, appropriate optimization of annealing conditions is important for overall performance of OPVs, and the optimum conditions

of annealing are different depending on the materials used in the active layer. It was reported that for P3HT:PCBM active layer appropriate annealing temperature is 150 °C, since it creates bicontinuous morphology quickly with crystalline polymers leading to enhancement in PCE.^[80] After annealing at this temperature, stable performance of OPVs is obtained. This indicates the formation of thermally stable nanoscale active layer.^[81] The use of additive such as DIO in this device assists to form a thin active layer that helps to improve exciton harvesting and charge separation active layer.^[82]

Yi et al.^[79] designed small molecule new donor molecule (DRDTSBDTT) and investigated their morphological and photovoltaic behavior under different annealing temperatures. **Figure 11A** shows that the optimal annealing temperature is at 80 °C with PCE of 5.05%. As the annealing temperature increases, V_{OC} drops from 1.02 to 0.96 V while both J_{SC} and FF increase until the optimal annealing temperature then decreases. TEM images provide a clear information about phase separation of active layer films annealed at different temperatures (see Figure 11B). As cast image shows a smooth surface, it is indicative of good solubility, and mixing happened without any noticeable phase separation. After annealing at 80 °C, a much better interpenetrating network was achieved with phase separation having a length scale of 20 nm. When the active layer film was annealed at 120 °C, clear phase separation could be spotted with a domain width of \approx 45 nm. Therefore, active layers

Table 7. OPVs performance in different solvents and additives.

Active layer ^{a)}	Solvent ^{b)}	Additive ^{c)}	μ_e [cm ² v ⁻¹ s ⁻¹]	μ_h [cm ² v ⁻¹ s ⁻¹]	μ_h/μ_e	PCE [%]	J_{SC} [mA cm ⁻²]	FF	V_{OC} [V]	References
PM6:Y6	CF	–	4.06×10^{-4}	3.09×10^{-4}	0.76	15.99	26.64	0.71	0.86	[133]
		DIB	4.41×10^{-4}	3.56×10^{-4}	0.81	16.63	27.46	0.74	0.84	
		DCT	4.87×10^{-4}	4.02×10^{-4}	0.83	16.80	27.12	0.75	0.85	
		DBT	5.63×10^{-4}	4.90×10^{-4}	0.87	17.29	27.32	0.75	0.85	
		DIT	6.97×10^{-4}	6.49×10^{-4}	0.93	17.48	27.59	0.75	0.85	
PBQx-TF:eC9-2Cl	Tol	–	1.25×10^{-4}	1.77×10^{-4}	1.42	16.90	25.90	0.73	0.89	[134]
		DIO	2.14×10^{-4}	2.64×10^{-4}	1.23	18.10	26.60	0.78	0.87	
		DCBB	3.55×10^{-4}	3.75×10^{-4}	1.06	19.20	27.20	0.80	0.88	
PM6:Y6	CF	–	2.91×10^{-4}	3.66×10^{-4}	1.26	15.31	24.22	0.72	0.85	[135]
		CN	7.44×10^{-4}	5.73×10^{-4}	0.77	15.87	24.69	0.74	0.84	
		2-HM	7.53×10^{-4}	7.83×10^{-4}	1.04	17.01	25.94	0.76	0.84	
PTB7-Th:IEICO-4F	CB	–	4.56×10^{-5}	9.35×10^{-5}	2.05	9.23	23.70	0.54	0.74	[136]
		1% CN	9.47×10^{-5}	1.26×10^{-4}	1.33	9.72	23.90	0.56	0.73	
		4% CN	1.48×10^{-4}	1.42×10^{-4}	0.95	12.1	26.80	0.66	0.71	
		7% CN	1.72×10^{-4}	1.56×10^{-4}	0.91	10.70	24.30	0.66	0.70	
PBDB-T:PC ₇₁ BM	CB	–	2.36×10^{-4}	3.66×10^{-4}	1.55	8.15	14.10	0.65	0.89	[137]
		1-THNO	4.13×10^{-4}	4.41×10^{-4}	1.07	9.36	15.14	0.71	0.87	
		THN	4.47×10^{-4}	4.54×10^{-4}	1.02	9.53	15.42	0.71	0.87	
PBDB-T:PF5-Y5	<i>o</i> -xylene	–	5.25×10^{-6}	5.80×10^{-5}	11.12	5.52	12.70	0.50	0.87	[138]
		CB	–	8.38×10^{-5}	1.36×10^{-4}	1.62	8.66	15.70	0.60	0.92
Y6:D18	Y6 CF:D18 CF	–	2.81×10^{-4}	3.11×10^{-4}	1.11	17.01	26.79	0.75	0.85	[139]
	Y6 CF:D18 CB	–	1.63×10^{-4}	2.53×10^{-4}	1.55	11.55	21.22	0.67	0.82	
	Y6 CB:D18 CF	–	2.66×10^{-6}	3.03×10^{-5}	1.14	17.00	26.97	0.74	0.85	
	Y6 CB:D18 CB	–	1.59×10^{-5}	2.26×10^{-4}	1.42	12.18	21.63	0.69	0.82	
PTB7-Th:ITIC	CB	–	1.10×10^{-4}	8.10×10^{-5}	0.74	7.41	13.88	0.66	0.80	[140]
	<i>o</i> -DCB	–	8.80×10^{-5}	5.90×10^{-5}	0.67	5.78	11.31	0.60	0.83	
	<i>o</i> -xylene	–	1.70×10^{-4}	9.00×10^{-5}	0.84	8.11	14.97	0.65	0.80	
	THF	–	7.10×10^{-5}	5.10×10^{-5}	0.72	6.79	14.14	0.59	0.81	

Abbreviations: ^{a)}PBQx-TF, Poly[(2,6-(4,8-bis(5-(2-ethylhexyl-3-fluoro)thiophen-2-yl)-benzo[1,2-b:4,5-b']dithiophene))-alt-5,5'-(6,9-bis(4-(2-butyloctyl)thiophen-2-yl)dithieno[3,2-f;2',3'-h]quinoxaline)]. eC9-2Cl, 2,2'-[[12,13-Bis(2-butyloctyl)-12,13-dihydro-3,9-dinonylbisthieno[2',3':4',5']thieno[2',3':4,5]pyrrolo[3,2-e:2',3'-g][1-3]benzothiadiazole-2,10-diyl]bis[methylidyne(2 or 3-chloro-3-oxo-1H-indene-2,1(3 H)-diylidene)]]]bis[propanedinitrile]. IEICO-4F, 2,2'-(2Z,2'Z)-(((4,4,9,9-tetrakis(4-hexylphenyl)-4,9-dihydro-sindaceno[1,2-b:5,6-b']dithiophene-2,7-diyl)bis(4-((2-ethylhexyl)oxy)thiophene-5,2-diyl))bis(methanonylidene))bis(5,6-difluoro-3-oxo-2,3-dihydro-1H-indene-2,1-diylidene))dimalononitrile; ^{b)}Tol, Toluene. THF, Tetrahydrofuran; ^{c)}DIB, 1,4-Diiodobenzene. DCT, 1,4-Dichlorothiophene. DBT, 1,4-Dibromothiophene. DIT, 2,5-Diiodothiophene. DIO, 1,8-Diiodooctane. DCBB, 3,5-Dichlorobromobenzene. CN, 1-chloronaphthalene. 2-HM, 2-hydroxy-4-methoxybenzophenone. 1-THNO, 1,2,3,4-Tetrahydronaphthalen-1-one. THN, 1,2,3,4-Tetrahydronaphthalene.

annealed at higher temperatures have larger phase separation and improved interpenetrating network. This is anticipated to have a negative effect on the electron–hole diffusion to the donor/acceptor interface. **The results shown in Table 9 reveal that the best performance of OPVs is achieved when the optimal annealing temperature is reached.** Different polymers used in the active layer have different optimal annealing temperatures depending on their structure and substituents. The μ_e and μ_h increase as the annealing temperature increases. After the optimal annealing temperature is reached, μ_e and μ_h decrease indicating the formation of larger phase separation, which turn causes a decrease in PCE.

4. Improving Stability of OPVs

Besides the PCE of the OPVs, the stability of the device is the main challenge that affects the commercialization of the OPVs. The materials used for the fabrication of the device determine the stability of the OPVs. To improve the stability of the organic active layer, which decides the lifetime of the device, the mechanisms of the degradation process taking place at the active layer need to be understood and provide the background of this process. Understanding this process will help with ideas on how materials can be modified sequentially to improve their stability. There are several challenges identified that are said to be

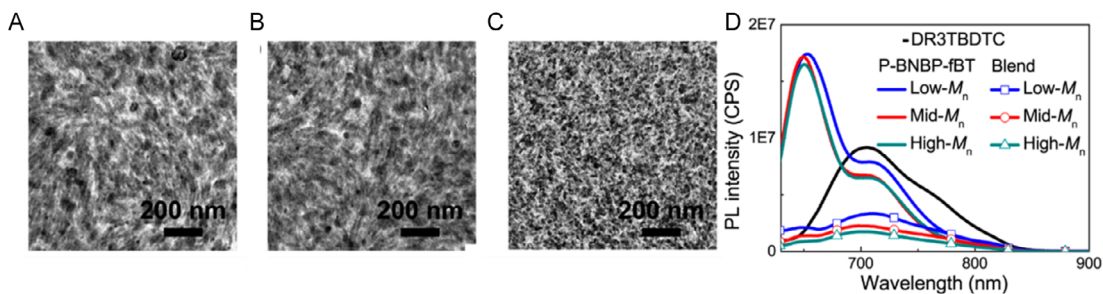


Figure 9. TEM images of DR3TBDTC:P-BNBP-fBT obtained from different molecular weights of P-BNBP-fBT polymers: A) DR3TBDTC:low-Mn P-BNBP-fBT, B) DR3TBDTC:mid-Mn P-BNBP-fBT, and C) DR3TBDTC:high-Mn P-BNBP-fBT. D) Photoluminescence showing comparison of DR3TBDTC, P-BNBP-fBT with different molecular weights and blends of DR3TBDTC:P-BNBP-fBT with different molecular weights. Reproduced with permission.^[76] Copyright 2019, American Chemical Society.

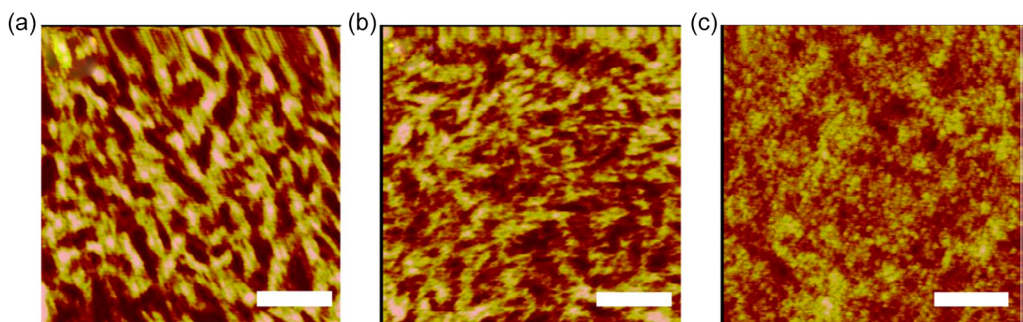


Figure 10. PPDT2FBT_L:P(NDI2OD-T2), PPDT2FBT_M:P(NDI2OD-T2), and PPDT2FBT_H:P(NDI2OD-T2) AFM images having rms roughness of 1.90, 1.20, and 0.80 nm, respectively. Reproduced with permission.^[77] Copyright 2015, American Chemical Society.

responsible for poor stability (short lifetime) of OPVs such as visible-near infrared light, UV light, moisture, and air.^[83] In the air, photo-oxidation of a crystalline polymer film takes place slower than amorphous film of similar materials because of the less chemically reactive ability due to the confinement of molecules.^[3,6,84] Oxygen can be conquered using encapsulations likewise to moisture. The use of encapsulation agents and UV filters can result in OPVs with a lifetime of over 15 years.^[85] In encapsulated OPVs, degradation is taking place around glass transition temperature (T_g). Above T_g , organic donor and acceptor materials can move leading to a blockage layer at the interface or an increase in the diffusion length causing FF to drop.^[86] Photodegradation in encapsulated OPVs takes place at the active layer because of the photochemical processes causing a decrease in V_{OC} .^[87] The photodegradation seems to be in relationship with the donor/acceptor interface. To improve the stability and performance of the OPVs, interfacial engineering is the main issue to address.

Recently, OPVs comprised either donor:acceptor:acceptor or donor:donor:acceptor as active layer have received a lot of attention. These types of OPVs are composed of three materials in the active layer and are termed ternary OPVs. The reason for studying ternary OPVs was to improve the PCE and stability. Yang et al.^[88] studied the photovoltaic response and stability test of donor:acceptor:acceptor using PM6 as donor material and Y6 and PIDTC-T as acceptor materials. They have obtained an efficiency of 16.76% and an improvement in stability. Their finding

revealed that the improved performance in terms of PCE and stability is due to the presence of PIDTC-T acceptor material, which led to enhancement in charge mobilities, reduced recombination, improved absorption, reasonable phase separation, and redistributed composition in active layers. He et al.^[89] reported addition of BTP-S9 in PM6:L8-BO OPV device for the consideration of aligned energy levels and complementary absorption spectrum. Their OPVs fabricated with and without BTP-S9 maintained 66% and 58% stability after 1000 h of illumination, respectively (see Figure 12A). To further confirm that the presence of BTP-S9 improves the stability of the OPVs, a photoaging study was performed under metal halide lamp illumination for 256 h in ambient conditions, as shown in Figure 12B. L8-BO is degraded when exposure time reaches 256 h, while BTP-S9 can still maintain its stability, and the L8-BO:BTP-S9 blend is much better than L8-BO because of BTP-S9 introduction. The higher stability due to the presence of BTP-S9 was attributed to its improved crystallinity leading to higher μ_e . Dong et al.^[90] investigated the use of benzo[1,2-b:4,5-b']dithiophene (BDT) as an additive into PM6:Y6 OPVs. The PCE of OPVs with and without BDT was obtained to be 16.30% and 17.91%, respectively. After stability studies were performed for 3000 h, 79.6% of OPV performance based on PCE of the device without BDT was retained, which is much lower than 90.0% of the BDT-processed device (see Figure 12C). Improved stability of BDT-processed device is due to enhanced molecular interaction between Y6 and BDT inducing ideal phase separation in the active layer, which improves exciton separation,

Table 8. Effect of molecular weight of donor and acceptor polymers on the performance of OPVs.

Donor ^d /Acceptor ^{a,a}	Molecular weight [kg mol ⁻¹]	μ_e [cm ² v ⁻¹ s ⁻¹]	μ_h [cm ² v ⁻¹ s ⁻¹]	ΔE_{LUMO} [eV]	E_g^{optical} [eV]	PCE [%]	J_{SC} [mA cm ⁻²]	FF	V_{OC} [V]	References
PTB7 ^d	28	—	2.85×10^{-4}	0.58	1.66	5.41	13.96	0.52	0.75	[141]
	40	—	4.20×10^{-4}	0.51	1.66	6.27	15.27	0.54	0.76	
	128	—	6.30×10^{-4}	0.26	1.62	8.50	18.51	0.60	0.76	
PTB7-Th ^d	50	—	0.62×10^{-2}	—	1.59	8.44	13.50	0.62	1.01	[71]
	100	—	0.78×10^{-2}	—	1.59	8.68	14.20	0.61	1.00	
	200	—	1.05×10^{-2}	—	1.59	9.57	15.20	0.63	1.00	
	300	—	1.16×10^{-2}	—	1.59	7.73	15.10	0.52	0.99	
P3HT ^d	35.90	—	9.80×10^{-5}	—	—	6.11	12.21	0.60	0.83	[142]
	6.0	—	7.10×10^{-5}	—	—	2.96	7.11	0.50	0.90	
PTzBI-Si ^d	15.40	—	6.61×10^{-3}	—	—	8.60	13.60	0.72	0.85	[143]
	58.20	—	6.73×10^{-3}	—	—	11.50	16.80	0.78	0.85	
PM6 ^d	134	—	4.00×10^{-4}	0.47	1.81	17.79	25.27	0.78	0.89	[144]
	142	—	4.10×10^{-4}	0.51	1.81	18.16	25.19	0.79	0.89	
	153	—	4.30×10^{-4}	0.50	1.81	18.04	25.16	0.79	0.89	
	164	—	3.80×10^{-4}	0.52	1.81	17.67	24.81	0.77	0.89	
DTBDT ^d	9.60	—	2.50×10^{-6}	0.09	1.72	0.85	2.00	0.45	0.94	[145]
	17.10	—	5.40×10^{-6}	0.07	1.69	1.25	3.50	0.40	0.89	
	32.00	—	2.60×10^{-5}	0.07	1.69	3.35	7.40	0.47	0.92	
	72.90	—	3.70×10^{-5}	0.05	1.67	4.10	9.90	0.45	0.89	
	138.90	—	3.80×10^{-5}	0.08	1.67	3.80	8.60	0.48	0.92	
PM6 ^d	9.90	—	9.17×10^{-6}	0.88	1.83	10.14	19.09	0.63	0.84	[146]
	11.58	—	5.87×10^{-4}	0.80	1.84	17.65	27.87	0.75	0.84	
	20.45	—	2.04×10^{-4}	0.60	1.72	14.75	25.44	0.68	0.86	
	21.82	—	2.24×10^{-4}	0.84	1.83	15.34	26.23	0.70	0.84	
PYT ^a	12.32	3.99×10^{-4}	—	0.01	1.38	16.86	24.64	0.74	0.93	[31]
	18.22	8.36×10^{-4}	—	0.03	1.35	15.83	24.62	0.74	0.87	
P-BNBP-fBT ^a	18.20	2.71×10^{-4}	—	0.51	1.89	3.08	5.46	0.53	1.06	[76]
	66.40	3.24×10^{-4}	—	0.52	1.87	4.21	7.00	0.56	1.08	
	117.30	4.10×10^{-4}	—	0.53	1.86	6.38	10.62	0.58	1.04	
P(NDI2OD-T2) ^a	15.20	1.90×10^{-6}	—	—	—	3.12	8.10	0.47	0.81	[147]
	20.50	2.50×10^{-6}	—	—	—	3.43	8.45	0.49	0.82	
	48.30	5.00×10^{-6}	—	—	—	4.24	9.87	0.52	0.82	
	103.50	7.10×10^{-6}	—	—	—	4.65	11.37	0.50	0.81	
	163.20	9.20×10^{-6}	—	—	—	4.96	12.90	0.47	0.81	

Abbreviation: ^{a)} PTzBI-Si, poly[(4,8-bis(5-(2-ethylhexyl) thiophen-2-yl)benzo[1,2-b:4,5-b']dithiophene-co-4,8-di(thien2-yl)-2-(6-(1,1,1,3,5,5,5-heptamethyltrisiloxan-3-yl)hexyl)-6-octyl][1-3]triazolo[4,5-f]isoindole-5,7(2H,6H)-dione]. DTBDT, Dithieno[2,3-d:2',3'-d']benzo[1,2-b:4,5-b']dithiophene. PYT, Poly[(2,20-((2Z,20Z)-((12,13-bis(2-octyldodecyl)-3,9-diundecyl-12,13-ihydro[1,2,5]thiadiazolo[3,4e]thieno[2'',3'':4',5']thieno[2',3':4,5]pyrrolo[3,2-g]thieno[2',3':4,5]thieno[3,2-b]indole-2,1'-diyl)bis(methanlylidene))bis(3-oxo-2,3-dihydro-1H-indene-2,1-diyldiene))dimalononitrile-alt-2,5-thiophene)]. P-BNBP-fBT, B-N bridged bipyridine-co-3, 3'-difluoro-2, 2'-bithiophene. PPDT2FBT, poly[(2,5-bis(2-hexyldecyloxy)phenylene)-alt-(5,6-difluoro-4,7-di(thienophen-2-yl)benzo[c][1,2,5]thiadiazole)]. P(NDI2OD-T2), Poly[[N,N'-bis(2-octyldodecyl)naphthalene-1,4,5,8-bis(dicarboximide)-2,6-diyl]-alt-5,5'-(2,2'-bithiophene)].

and charge transfer and decreases bimolecular recombination. Therefore, this study revealed that developing and combining novel materials and device engineering give a way toward highly efficient and more stable OPVs. **Table 10** shows the studies

reported on improved stability of OPVs by the addition of a third component. After the addition of a third component, photovoltaic parameters such as PCE, J_{SC} , V_{OC} , and FF increase significantly along with stability.

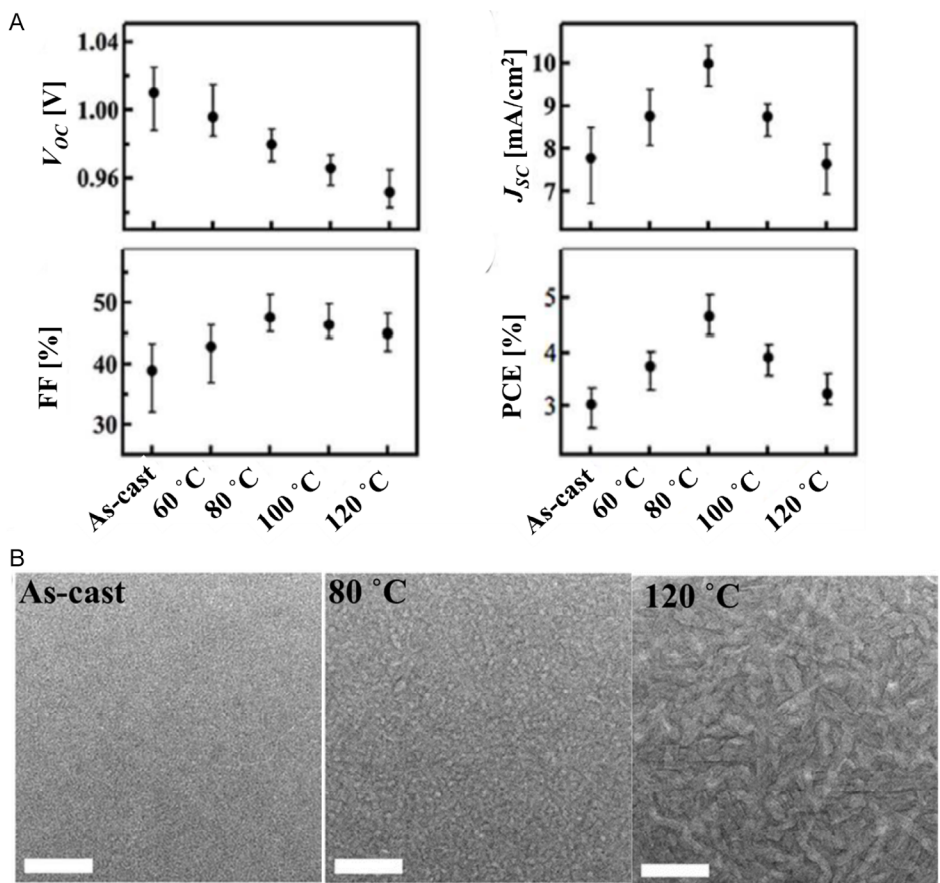


Figure 11. A) V_{OC} , J_{SC} , FF, and PCE plots against annealing temperature for DRDTSBDTT:PC₇₁BM devices. B) Transmission electron microscope images of DRDTSBDTT:PC₇₁BM as-cast, annealed at 80 and 120 °C. Reproduced with permission.^[79] Copyright 2014, The Royal Society of Chemistry.

5. Conclusion

In this work, we outlined the processes that are taking place in OPVs. Understanding how OPVs work can help with developing new donor and acceptor materials with improved photovoltaic properties. Studying how OPVs processes such as light absorption, exciton diffusion, exciton dissociation/separation, charge transportation, and charge collection are affected by substituents on the donor and acceptor materials together with incorporation of nanoparticles in the active layer can guide on how to improve the performance of OPVs. As discussed in this work, there are several ways to improve the OPVs processes: 1) the incorporation of nanoparticles in the active layer turns to increase the light absorption by introducing new absorption bands, increasing the absorbance, and causing a red-shift of the existing absorption bands. However, incorporation of too high concentration of nanoparticles causes a blue shift and decrease in absorbance on UV-vis spectrum. Substitution of electron-withdrawing groups on the nonfullerene acceptors also improves the light absorption in the active layer. 2) Charge diffusion can be improved by introduction of heavy atoms on the structure of active layer materials and introduction of third component in an active layer. The presence of heavy atoms and hydrophilic

third component improves the charge diffusion by increasing the lifetime of electron–hole pair. The position of substituents on either donor or acceptor material affects the diffusion length of charges. 3) The use of bridging material in a binary active layer significantly improves the electron–hole dissociation by decreasing the ΔE_{LUMO} . They will reduce the recombination rate of electrons and holes after dissociation by increasing the η_{diss} . 4) Charge transportation can be improved by functionalization of donor and acceptor materials using alkyl chains. There is no trend between the length of alkyl chain and the charge transportation efficiency. The various structures of the central core also play a crucial role in charge transportation since their morphology is tailored differently with different side chains. 5) Introduction of hole and electron transport layers between the active layer and electrodes increases the efficiency of charge collection from the active layer. The conductivity of charge collection layers can be increased by incorporate of metallic nanoparticles. Incorporation of high concentration of nanoparticles reduces conductivity by formation of aggregates resulting in weaker phase separation.

We also reviewed factors that affect the performance of OPVs such as active layer thickness, solvents and additives, molecular weight of donor material, and annealing temperature. It is

Table 9. Effect of temperature conditions on the performance of OPVs.

Active layer ^{a)}	Annealing conditions		μ_e [$\text{cm}^2 \text{V}^{-1} \text{s}^{-1}$]	μ_h [$\text{cm}^2 \text{V}^{-1} \text{s}^{-1}$]	PCE [%]	J_{SC} [mA cm^{-2}]	FF	V_{OC} [V]	References
	Temperature [°C]	Time [min]							
PM6:Y6	100	10	6.47×10^{-4}	9.46×10^{-4}	15.91	25.58	0.72	0.85	[148]
	120		10.41×10^{-4}	13.50×10^{-4}	16.71	25.78	0.75	0.85	
	150		16.58×10^{-4}	19.61×10^{-4}	17.36	26.16	0.76	0.86	
	180		2.58×10^{-4}	3.93×10^{-4}	15.68	25.30	0.71	0.85	
PM6:Y6	—	5	3.53×10^{-4}	5.42×10^{-4}	16.06	25.33	0.74	0.85	[149]
	60		4.89×10^{-4}	6.99×10^{-4}	16.44	26.09	0.75	0.84	
	80		7.08×10^{-4}	9.23×10^{-4}	16.88	26.52	0.76	0.84	
	100		5.98×10^{-4}	8.33×10^{-4}	16.50	26.22	0.76	0.83	
PBDB-T-Cl:PBI	25	10	1.70×10^{-4}	5.80×10^{-4}	4.30	9.90	0.46	0.95	[150]
	100		2.10×10^{-6}	1.40×10^{-3}	4.60	9.80	0.50	0.94	
	150		1.40×10^{-6}	1.00×10^{-3}	5.00	10.30	0.52	0.94	
	200		1.10×10^{-4}	7.50×10^{-2}	5.70	10.60	0.58	0.92	
	230		2.10×10^{-4}	0.26	6.30	10.80	0.65	0.90	
	280		2.70×10^{-4}	0.33	4.60	9.80	0.53	0.88	
PDCBT-Cl:Y6	—	10	1.30×10^{-5}	5.00×10^{-5}	0.10	0.45	0.25	0.93	[151]
	120		1.90×10^{-5}	5.60×10^{-5}	1.22	4.86	0.28	0.91	
	130		2.70×10^{-5}	6.50×10^{-5}	2.91	10.77	0.31	0.88	
	140		4.40×10^{-5}	6.70×10^{-5}	5.07	14.95	0.38	0.88	
	150		4.60×10^{-5}	7.30×10^{-5}	7.53	18.60	0.46	0.88	
	160		10.00×10^{-5}	8.60×10^{-5}	9.79	22.18	0.51	0.86	
	170		6.00×10^{-5}	8.20×10^{-5}	8.78	20.01	0.52	0.84	
	180		5.60×10^{-5}	3.70×10^{-5}	8.43	20.09	0.52	0.81	
PffBT4T-2OD:PC ₇₁ BM	—	5	5.93×10^{-5}	—	7.17	15.45	0.64	0.73	[152]
	60		4.02×10^{-4}	—	8.01	15.98	0.68	0.74	
	80		5.35×10^{-4}	—	8.56	17.04	0.67	0.75	
	100		3.19×10^{-4}	—	7.55	15.54	0.64	0.76	
	120		1.73×10^{-4}	—	7.11	15.76	0.58	0.78	
	140		2.62×10^{-4}	—	5.93	13.02	0.58	0.78	
	—	10	0.07×10^{-4}	1.29×10^{-4}	5.74	13.16	0.48	0.92	[153]
DRTT-R:N3	110		0.78×10^{-4}	1.67×10^{-4}	7.11	15.90	0.51	0.89	
	120		1.11×10^{-4}	1.51×10^{-4}	7.52	15.73	0.56	0.89	
	130		1.22×10^{-4}	1.30×10^{-4}	7.74	15.78	0.56	0.88	
	140		1.07×10^{-4}	1.25×10^{-4}	7.57	15.46	0.54	0.88	
	—	10	0.24×10^{-4}	0.90×10^{-4}	6.44	15.09	0.48	0.90	
DRTT-T:N3	90		0.92×10^{-4}	1.51×10^{-4}	9.52	18.35	0.60	0.89	
	100		1.17×10^{-4}	1.10×10^{-4}	11.84	20.68	0.65	0.88	
	110		0.91×10^{-4}	0.91×10^{-4}	11.63	20.79	0.65	0.87	
	—	10	0.42×10^{-4}	1.50×10^{-4}	7.69	17.63	0.49	0.89	
DRTT-2T:N3	90		0.79×10^{-4}	1.70×10^{-4}	9.01	19.28	0.54	0.88	
	100		1.29×10^{-4}	1.83×10^{-4}	10.22	20.82	0.57	0.86	
	110		1.60×10^{-4}	1.65×10^{-4}	10.86	21.37	0.60	0.85	
	120		1.34×10^{-4}	1.19×10^{-4}	9.13	20.07	0.55	0.83	
	—	10	0.66×10^{-4}	1.47×10^{-4}	7.46	17.13	0.49	0.90	
DRTT-TT:N3	110		0.75×10^{-4}	1.97×10^{-4}	8.01	18.10	0.50	0.90	
	120		1.14×10^{-4}	1.63×10^{-4}	9.07	19.82	0.53	0.88	

Table 9. Continued.

Active layer ^{a)}	Annealing conditions		μ_e [cm ² v ⁻¹ s ⁻¹]	μ_h [cm ² v ⁻¹ s ⁻¹]	PCE [%]	J_{SC} [mA cm ⁻²]	FF	V_{OC} [V]	References
	Temperature [°C]	Time [min]							
	130		1.35×10^{-4}	1.38×10^{-4}	9.91	21.12	0.55	0.85	
	140		1.13×10^{-4}	1.19×10^{-4}	8.12	19.60	0.50	0.82	

Abbreviation: ^{a)}PBDB-T-Cl, Poly[(2,6-(4,8-bis(5-(2-ethylhexyl-3-chloro)thiophen-2-yl)-benzo[1,2-b:4,5-b']dithiophene))-alt-(5,5-(1',3'-di-2-thienyl-5',7'-bis(2-ethylhexyl)benzo[1',2'-c:4',5'-c']dithiophene-4,8-dione))]. PBI, Perylene bisimide. PDCBT-Cl, Poly[5,5'-bis(2-hexyldecyl)-(2,2'-bithiophene)-4,4'-dicarboxylate-alt-5,5'-3-chloro-2,2'-bithiophene]. PffBT4T-2OD, Poly[(5,6-difluoro-2,1,3-benzothiadiazol-4,7-diyl)-alt-(3,3'''-di(2-octyldodecyl)-2,2';5',2'';5",2'''-quaterthiophen-5,5'''-diyl)].

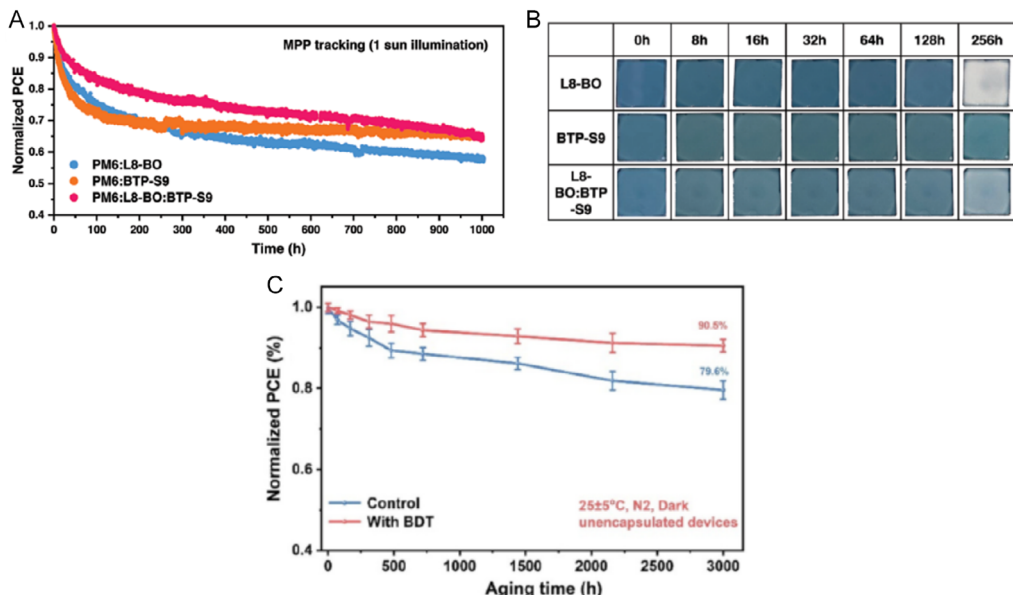


Figure 12. A) Stability comparison of OPV devices with and without BTP-S9 and B) digital photos comparing the photoaging process of acceptor materials. Reproduced with permission.^[89] Copyright 2023, John Wiley & Sons—Books. C) Stability of OPVs processed with and without BDT. Reproduced with permission.^[90] Copyright 2024, John Wiley & Sons—Books.

difficult to tune those factors since they are very sensitive and as new materials are developed, the optimal conditions consequently change. Further understanding of how those factors change as the structure of a donor or acceptor material changes is still required. As the thickness of the active layer increases, the photovoltaic parameters are affected. According to the studies reviewed in this work, most active layers perform better in OPVs with a thickness of 100 nm. Most balanced charge transport is achieved at this thickness resulting in a decrease in charge recombination. At a higher thickness of the active layer, charge recombination is promoted because of an increase in diffusion length. The presence of additives in an active layer helps to tune the morphology and improve the charge transport within the active layer. Solvents with higher boiling point helps in improving the crystallinity of the active layer. The μ_h and μ_e mobilities increase as the molecular weight of donor and acceptor increases, respectively. Donor materials have an optimal molecular weight

depending on the chemical structure according to the studies reported in this work. As the molecular weight of either donor or acceptor material changes, there is a slight change in the optical bandgap and ΔE_{LUMO} . The annealing temperature of OPVs changes the morphology of the active layer as it increases. After optimal annealing temperature is reached, larger phase separation is obtained with reduced charge transportation to the interface. Polymers with different structures and substituents have different optimal annealing temperatures for better OPVs performance.

The stability of OPVs has been successfully improved by incorporation of third component in an active layer. This third component also facilitates electron-hole separation, charge transportation, and reduction of charge recombination. The development of photochemical and thermally stable polymers is crucial to achieve better lifetimes that can compete with that of inorganic materials-based photovoltaic cells. Developing new

Table 10. Effect of the third component on the stability of OPVs.

Active layer	Third component ^{a)}	PCE [%]	J_{SC} [mA cm^{-2}]	FF	V_{OC} [V]	Time after initial efficiency [h]	Retained PCE [%]	References
PM6:Y6	–	16.31	26.06	0.74	0.85	1200	91.00	[154]
	PCN3	17.44	26.65	0.77	0.85			
PBDB-T:ITI	–	10.27	16.55	0.69	0.90	2880	67.30	[50]
	AST	12.07	17.86	0.73	0.93			
PBDB-T:PYF-T	–	10.27	18.02	0.68	0.84	144	79.75	[155]
	PZT	16.37	25.09	0.76	0.86			
PM6:Y6	–	17.41	26.95	0.75	0.86	1800	89.00	[156]
	dT9TBO	18.41	27.17	0.77	0.88			
D18-Cl:N3	–	16.54	26.74	0.72	0.86	500	94.00	[103]
	BTR-Cl	17.92	27.92	0.75	0.86			
PM6:Y6	–	15.78	25.41	0.72	0.86	2000	79.00	[157]
	TIT-2Cl	18.18	26.63	0.78	0.88			
PM6:PC ₇₁ BM	–	8.37	11.77	0.74	0.96	1440	32.00	[158]
	BDT – 2TiC16 – 2CN	9.39	12.98	0.76	0.96			
PM6:Y6	–	15.60	25.88	0.72	0.83	1080	85.34	[159]
	IDIC-C4Ph	18.10	26.65	0.78	0.87			
PTB7:PC ₆₁ BM	–	7.60	15.51	0.67	0.74	680	88.00	[160]
	10% PDI-DPP-PDI	8.71	15.95	0.70	0.78			
	20% PDI-DPP-PDI	6.85	13.33	0.65	0.80			
	30% PDI-DPP-PDI	5.97	12.40	0.62	0.78			
PM6:L8-BO	–	18.30	25.91	0.80	0.89	200	77.00	[161]
	Y-SeNF	19.28	27.88	0.79	0.87			
D18:N3	–	18.16	27.98	0.78	0.83	476	49.00	[162]
	QX- α	19.33	27.86	0.80	0.86			
PM6:Y6	–	15.62	25.44	0.72	0.84	2	77.00	[163]
	UV329	16.65	26.56	0.74	0.84			
PM6:BTP-eC9	–	17.90	26.29	0.77	0.86	300	60.00	[164]
	isoIDTIC	19.00	26.64	0.80	0.87			
PBQx-TCl:PY-IT	–	17.84	24.18	0.78	0.95	1400	50.00	[165]
	PY-IV	18.81	25.25	0.79	0.94			
16PTB7-Th:Y6	–	7.71	20.16	0.57	0.67	880	60.00	[166]
	PC ₇₁ BM	9.55	24.68	0.58	0.67			
PM6:Y6	–	15.70	25.10	0.73	0.86	1500	63.00	[167]
	MOITIC	17.10	25.60	0.76	0.88			
PM6:Y6	–	15.20	25.10	0.73	0.83	110	60.00	[168]
	O-IDTBR	16.60	25.75	0.76	0.85			

Abbreviation: ^{a)}PDI-DPP-PDI, Perylenediimide-Diketopyrrolopyrrole-Perylenediimide. dT9TBO, 1,6-bis[2,2'-(2Z,2'Z)-((12,13-bis(2-ethylhexyl)-3,9-dinonanyl-12,13-dihydro-1,2,5]thiadiazolo[3,4-e]thieno[2",3":4',5']thieno[2',3":4,5]pyrrolo[3,2g]thieno[2',3":4,5]thieno[3,2-b]indole-2,10-diy)bis(methanylidene))bis(5-thienyl-3-oxo-2,3-dihydro-1H-indene-2,1-diydene))dimalononitrile]hexane. IDIC-C4Ph, 6,6-, 12,12-tetrakis(4-benzylbutyl)-s-indaceno[3,2-b]thiophene-bis(2-(6-methyl-3-oxo-2,3-dihydro-1H-inden-1-ylidene)malononitrile). UV329, 2-(2-hydroxy-5-tert-octylphenyl)benzotriazole.

materials for OPVs requires proper optimization studies for a better understanding of the overall performance. Processing with nonhalogenated solvents and treatment with nonhalogenated additives must be considered to fabricate OPVs with green additives and solvents for their future application.

Acknowledgements

The authors most gratefully acknowledge the financial support of the University Research Committee of the University of Cape Town (ID: 1524665) and the National Research Foundation of South Africa (grant no. PSTD2204062241).

Conflict of Interest

The authors declare no conflict of interest.

Keywords

active layer processes, organic photovoltaic cells optimization, organic donor/acceptor materials and stability, organic photovoltaic cells

Received: November 28, 2023

Revised: January 25, 2024

Published online: March 4, 2024

- [1] M. Yang, S. Fu, L. Wang, M. Ren, H. Li, S. Han, X. Lu, F. Lu, J. Tong, J. Li, *Opt. Mater.* **2023**, *137*, 113503.
- [2] Y. Wang, Z. Zheng, J. Wang, X. Liu, J. Ren, C. An, S. Zhang, J. Hou, *Adv. Mater.* **2023**, *35*, 2208305.
- [3] M. E. Ramoroka, S. B. Mdluli, V. S. John-Denk, K. D. Modibane, C. J. Arendse, E. I. Iwuoha, *Polymers* **2020**, *13*, 2.
- [4] C. Han, J. Wang, S. Zhang, L. Chen, F. Bi, J. Wang, C. Yang, P. Wang, Y. Li, X. Bao, *Adv. Mater.* **2023**, *35*, 2208986.
- [5] L. Huo, T. Liu, X. Sun, Y. Cai, A. J. Heeger, Y. Sun, *Adv. Mater.* **2023**, *27*, 2938.
- [6] M. E. Ramoroka, S. B. Mdluli, V. S. John-Denk, K. C. Januarie, K. D. Modibane, K. C. Nwambaekwe, S. T. Yussuf, K. V. Mokwebo, A. R. Williams, E. I. Iwuoha, *Front. Mater. Sci.* **2022**, *9*, 255.
- [7] Z. Wang, Z. Li, J. Liu, J. Mei, K. Li, Y. Li, Q. Peng, *ACS Appl. Mater. Interfaces* **2016**, *8*, 11639.
- [8] K. C. Nwambaekwe, M. E. Ramoroka, E. I. Iwuoha, *J. Sci. Adv. Mater. Dev.* **2023**, *8*, 100553.
- [9] S. T. Yussuf, M. E. Ramoroka, S. B. Mdluli, K. C. Nwambaekwe, P. I. Ekwere, O. V. Uhuo, C. O. Ikpo, E. I. Iwuoha, *J. Alloys Compd.* **2023**, *935*, 168211.
- [10] S. T. Yussuf, K. C. Nwambaekwe, M. E. Ramoroka, E. I. Iwuoha, *Mater. Today Sustainability* **2022**, *21*, 100287.
- [11] L. Kong, Z. Zhang, N. Zhao, Z. Cai, J. Zhang, M. Luo, X. Wang, M. Chen, W. Zhang, L. Zhang, Z. Wei, *Adv. Energy Mater.* **2023**, *13*, 2300763.
- [12] G. Ding, T. Chen, M. Wang, X. Xia, C. He, X. Zheng, Y. Li, D. Zhou, X. Lu, L. Zuo, Z. Xu, *Nanomicro. Lett.* **2023**, *15*, 92.
- [13] C. Sun, C. Zhu, L. Meng, Y. Li, *Adv. Mater.* **2022**, *34*, 2104161.
- [14] J. Jin, Q. Wang, K. Ma, W. Shen, L. A. Belfiore, X. Bao, J. Tang, *Adv. Funct. Mater.* **2023**, *33*, 2213324.
- [15] Z. Li, X. Li, J. Xue, J. Zhang, C. Zhu, J. Li, W. Ma, L. Meng, Y. Li, *ACS Energy Lett.* **2023**, *8*, 2488.
- [16] J. Zhu, R. Hao, J. Wang, D. Sun, X. Song, M. Zhu, B. Zhang, Y. Liu, H. Tan, W. Zhu, *Dyes Pigm.* **2022**, *210*, 111003.
- [17] K. Ma, W. Feng, H. Liang, H. Chen, Y. Wang, X. Wan, Z. Yao, C. Li, B. Kan, Y. Chen, *Adv. Funct. Mater.* **2023**, *33*, 2214926.
- [18] H. Gao, Y. Sun, L. Meng, C. Han, X. Wan, Y. Chen, *Small* **2023**, *19*, 2205594.
- [19] J. Wang, D. Qian, F. Dong, H. Wu, H. Pan, S. Liang, H. Wu, X. Feng, W. Li, M. Wang, Z. Tang, *Chem. Eng. J.* **2023**, *465*, 142909.
- [20] S. Kim, K. P. Hong, M. A. Saeed, T. H. Kim, H. Ahn, W. Lee, J. W. Shim, Y. H. Kim, *Appl. Surf. Sci.* **2023**, *623*, 157140.
- [21] N. Yang, T. Zhang, S. Wang, C. An, S. Seibt, G. Wang, J. Wang, Y. Yang, W. Wang, Y. Xiao, H. Yao, *Small Methods* **2023**, *8*, 2300036.
- [22] K. Hu, C. Zhu, S. Qin, W. Lai, J. Du, L. Meng, Z. Zhang, Y. Li, *Sci. Bull.* **2022**, *67*, 2096.
- [23] L. Zeng, R. Ma, Z. Zhou, T. Liu, Y. Xiao, X. Lu, D. Xue, W. Zhu, H. Yan, Y. Liu, *Chem. Eng. J.* **2022**, *429*, 132551.
- [24] X. Wang, Z. Li, X. Zheng, C. Xiao, T. Hu, Y. Liao, R. Yang, *Adv. Funct. Mater.* **2023**, *33*, 2300323.
- [25] G. H. Kim, C. Lee, K. Kim, D. H. Ko, *Nano Energy* **2023**, *106*, 108108.
- [26] M. Zhou, C. Liao, Y. Duan, X. Xu, L. Yu, R. Li, Q. Peng, *Adv. Mater.* **2023**, *35*, 2208279.
- [27] B. Zhang, F. Yang, Y. Li, *Small Sci.* **2023**, *3*, 2300004.
- [28] J. W. Yoon, H. Bae, J. Yang, J. W. Ha, C. Lee, J. Lee, S. C. Yoon, H. Choi, S. J. Ko, *Chem. Eng. J.* **2023**, *452*, 139423.
- [29] F. Meng, Y. Qin, Y. Zheng, Z. Zhao, Y. Sun, Y. Yang, K. Gao, D. Zhao, *Angew. Chem.* **2023**, *135*, e202217173.
- [30] R. Suthar, H. Dahya, S. Karak, G. D. Sharma, *Energy Technol.* **2023**, *11*, 2201176.
- [31] X. Wu, X. Yang, Y. Shao, Y. Gao, J. Wan, S. Ponomarenko, Y. Luponosov, R. Sun, J. Min, *Sol. RRL* **2023**, *7*, 2300064.
- [32] X. M. Huang, N. Chen, D. N. Ye, A. G. Zhong, H. Liu, Z. Li, S. Y. Liu, *Sol. RRL* **2023**, *7*, 2300143.
- [33] A. G. Waketola, F. G. Hone, G. T. Mola, S. O. Oseni, H. Ogutu, N. A. Tegegne, *Appl. Phys. A* **2023**, *129*, 96.
- [34] S. Liu, Y. Sun, L. Chen, Q. Zhang, X. Li, J. Shuai, *Mater. Today Phys.* **2022**, *24*, 100680.
- [35] Z. Du, T. Yu, W. He, A. Yurtsever, R. Izquierdo, M. Jafari, M. Siaj, D. Ma, *ACS Appl. Mater. Interfaces* **2022**, *14*, 16185.
- [36] X. Liao, Q. Li, J. Ye, Z. Li, J. Ren, K. Zhang, Y. Xu, Y. P. Cai, S. Liu, F. Huang, *Chem. Eng. J.* **2023**, *453*, 139489.
- [37] B. Basha, T. Mubashir, M. H. Tahir, J. Najeeb, S. Naeem, Z. A. Alrowaili, M. S. Al-Buraihi, *Inorg. Chem. Commun.* **2023**, *153*, 110818.
- [38] X. Ma, W. Xu, Z. Liu, S. Y. Jeong, C. Xu, J. Zhang, H. Y. Woo, Z. Zhou, F. Zhang, *ACS Appl. Mater. Interfaces* **2023**, *15*, 7247.
- [39] W. Farooq, A. Alzahrani, S. S. Ghoneim, *J. Comput. Electron.* **2023**, *22*, 867.
- [40] M. S. Kumar, K. Balachander, *Optik* **2016**, *127*, 2725.
- [41] C. Yang, C. Zhao, Y. Sun, Q. Li, M. R. Islam, K. Liu, Z. Wang, S. Qu, Z. Wang, *Carbon Energy* **2021**, *3*, 4.
- [42] A. Y. Ahmed, J. N. Ike, M. S. Hamed, G. T. Mola, *J. Appl. Polym. Sci.* **2023**, *140*, e53697.
- [43] M. Deng, X. Xu, Y. Duan, L. Yu, R. Li, Q. Peng, *Adv. Mater.* **2023**, *35*, 2210760.
- [44] S. S. Alarfaji, F. Rasool, B. Iqbal, A. Hussain, R. Hussain, M. Akhlaq, M. F. U. Rehman, *ACS Omega* **2023**, *8*, 4767.
- [45] M. T. Sajjad, A. Ruseckas, L. K. Jagadamma, Y. Zhang, I. D. Samuel, *J. Mater. Chem. A* **2020**, *8*, 15687.
- [46] Y. Tamai, H. Ohkita, H. Benten, S. Ito, *J. Phys. Chem. Lett.* **2015**, *6*, 3417.
- [47] B. T. Luppi, D. Majak, M. Gupta, E. Rivard, K. Shankar, *J. Mater. Chem. A* **2019**, *7*, 2445.
- [48] T. Yang, A. Zhou, Y. He, Z. Yao, X. Song, X. Tao, Y. Tao, *Mater. Adv.* **2023**, *4*, 631.
- [49] V. S. Gevaerts, E. M. Herzog, M. Kirkus, K. H. Hendriks, M. M. Wient, J. Perlich, P. Müller-Buschbaum, R. A. Janssen, *Chem. Mater.* **2014**, *26*, 916.
- [50] J. Huang, H. Yu, *Electrochim. Acta* **2023**, *439*, 141684.
- [51] S. Athanasopoulos, S. Tscheuschner, H. Bässler, A. Köhler, *J. Phys. Chem. Lett.* **2017**, *8*, 2093.
- [52] A. Karki, J. Vollbrecht, A. J. Gillett, S. S. Xiao, Y. Yang, Z. Peng, N. Schopp, A. L. Dixon, S. Yoon, M. Schrock, H. Ade, *Energy Environ. Sci.* **2020**, *13*, 3679.
- [53] K. M. Pelzer, S. B. Darling, *Mol. Syst. Des. Eng.* **2016**, *1*, 10.
- [54] B. Park, H. Bae, J. W. Ha, C. Lee, J. Lee, Y. Heo, B. Kim, S. C. Yoon, H. Choi, S. J. Ko, *Org. Electron.* **2023**, *113*, 106717.

- [55] D. Mo, H. Chen, J. Zhou, N. Tang, L. Han, Y. Zhu, P. Chao, H. Lai, Z. Xie, F. He, *J. Mater. Chem. A* **2020**, *8*, 8903.
- [56] X. Wang, C. Xiao, X. Sun, A. Saparbaev, S. Lei, M. Zhang, T. Zhong, Z. Li, J. Zhang, M. Zhang, Y. Yu, *Nano Energy* **2022**, *101*, 107538.
- [57] H. J. Son, H. K. Park, J. Y. Moon, B. K. Ju, S. H. Kim, *Sustainable Energy Fuels* **2020**, *4*, 1974.
- [58] C. Hou, H. Yu, *J. Mater. Chem. C* **2020**, *8*, 4169.
- [59] X. Fan, W. Song, T. Lei, B. Xu, F. Yan, N. Wang, H. Cui, Z. Ge, *Mater. Chem. Front.* **2019**, *3*, 901.
- [60] M. Wang, Y. Sun, J. Guo, Z. Li, C. Liu, W. Guo, *Org. Electron.* **2019**, *74*, 258.
- [61] P. Morvillo, E. Bobeico, S. Esposito, R. Diana, *Energy Proc.* **2012**, *31*, 69.
- [62] Y. Zang, Q. Xin, J. Zhao, J. Lin, *J. Phys. Chem. C* **2018**, *122*, 16532.
- [63] W. Yang, W. Wang, Y. Wang, R. Sun, J. Guo, H. Li, M. Shi, J. Guo, Y. Wu, T. Wang, G. Lu, *Joule* **2021**, *5*, 1209.
- [64] L. Zhang, H. Zhao, B. Lin, J. Yuan, X. Xu, J. Wu, K. Zhou, X. Guo, M. Zhang, W. Ma, *J. Mater. Chem. A* **2019**, *7*, 22265.
- [65] S. Pang, Z. Chen, J. Li, Y. Chen, Z. Liu, H. Wu, C. Duan, F. Huang, Y. Cao, *Mater. Horiz.* **2023**, *10*, 473.
- [66] R. Zhao, Y. Li, Z. Ding, Z. Wu, H. Y. Woo, K. Zhao, X. Wang, S. F. Liu, Y. Li, *Macromolecules* **2023**, *56*, 867.
- [67] J. Jo, S. I. Na, S. S. Kim, T. W. Lee, Y. Chung, S. J. Kang, D. Vak, D. Y. Kim, *Adv. Funct. Mater.* **2009**, *19*, 2398.
- [68] U. Vongsaysy, D. M. Bassani, L. Servant, B. Pavageau, G. Wantz, H. Aziz, *J. Photonics Energy* **2014**, *4*, 040998.
- [69] B. Xu, G. Sai-Anand, A. I. Gopalan, Q. Qiao, S. W. Kang, *Polymers* **2018**, *10*, 121.
- [70] X. J. Zhou, T. T. Dai, X. Li, Y. J. Yan, W. Xiong, T. Lin, J. Zhou, D. H. Xu, Y. H. Zhu, J. Zhao, A. C. Geng, *ACS Appl. Energy Mater.* **2021**, *4*, 8175.
- [71] S. F. Hoefler, T. Rath, N. Pastukhova, E. Pavlica, D. Scheunemann, S. Wilken, B. Kunert, R. Resel, M. Hobisch, S. Xiao, G. Bratina, *J. Mater. Chem. A* **2018**, *6*, 9506.
- [72] D. Spoltore, T. Vangerven, P. Verstappen, F. Piersimon, S. Bertho, K. Vandewal, N. Van den Brande, M. Defour, B. Van Mele, A. De Sio, J. Parisi, *Org. Electron.* **2015**, *21*, 160.
- [73] Z. Ding, J. Kettle, M. Horie, S. W. Chang, G. C. Smith, A. I. Shames, E. A. Katz, *J. Mater. Chem. A* **2016**, *4*, 7274.
- [74] X. He, B. Cao, T. C. Hauger, M. Kang, S. Gusalov, E. J. Luber, J. M. Buriak, *ACS Appl. Mater. Interfaces* **2015**, *7*, 8188.
- [75] A. T. Yiu, P. M. Beaujuge, O. P. Lee, C. H. Woo, M. F. Toney, J. M. Frechet, *J. Am. Chem. Soc.* **2012**, *134*, 2180.
- [76] Z. Zhang, T. Wang, Z. Ding, J. Miao, J. Wang, C. Dou, B. Meng, J. Liu, L. Wang, *Macromolecules* **2019**, *52*, 8682.
- [77] H. Kang, M. A. Uddin, C. Lee, K. H. Kim, T. L. Nguyen, W. Lee, Y. Li, C. Wang, H. Y. Woo, B. J. Kim, *J. Am. Chem. Soc.* **2015**, *137*, 2359.
- [78] A. Bagui, V. Gupta, K. K. Maurya, S. P. Singh, *J. Phys. Chem. C* **2016**, *120*, 24615.
- [79] Z. Yi, W. Ni, Q. Zhang, M. Li, B. Kan, X. Wan, Y. Chen, *J. Mater. Chem. C* **2014**, *2*, 7247.
- [80] M. Milanovich, T. Sarkar, Y. Popowski, J. Z. Low, L. M. Campos, S. Kenig, G. L. Frey, E. Amir, *J. Mater. Chem. C* **2020**, *8*, 7698.
- [81] J. Liu, X. Zhu, J. Li, J. Shen, G. Tu, *RSC Adv.* **2016**, *6*, 61934.
- [82] B. A. Collins, Z. Li, J. R. Tumbleston, E. Gann, C. R. McNeill, H. Ade, *Adv. Energy Mater.* **2013**, *3*, 65.
- [83] R. Cheacharoen, W. R. Mateker, Q. Zhang, B. Kan, D. Sarkisian, X. Liu, J. A. Love, X. Wan, Y. Chen, T. Q. Nguyen, G. C. Bazan, *Sol. Energy Mater. Sol. Cells* **2017**, *161*, 368.
- [84] W. R. Mateker, T. Heumueller, R. Cheacharoen, I. T. Sachs-Quintana, M. D. McGehee, J. Warnan, P. M. Beaujuge, X. Liu, G. C. Bazan, *Chem. Mater.* **2015**, *27*, 6345.
- [85] W. R. Mateker, I. T. Sachs-Quintana, G. F. Burkhard, R. Cheacharoen, M. D. McGehee, *Chem. Mater.* **2015**, *27*, 404.
- [86] I. T. Sachs-Quintana, T. Heumueller, W. R. Mateker, D. E. Orozco, R. Cheacharoen, S. Sweetnam, C. J. Brabec, M. D. McGehee, *Adv. Funct. Mater.* **2014**, *24*, 3978.
- [87] I. Fraga Dominguez, P. D. Topham, P. O. Bussiere, D. Begue, A. Rivaton, *J. Phys. Chem. C* **2015**, *119*, 2166.
- [88] T. Yang, R. Ma, H. Cheng, Y. Xiao, Z. Luo, Y. Chen, S. Luo, T. Liu, X. Lu, H. Yan, *J. Mater. Chem. A* **2020**, *8*, 17706.
- [89] C. He, Q. Shen, B. Wu, Y. Gao, S. Li, J. Min, W. Ma, L. Zuo, H. Chen, *Adv. Energy Mater.* **2023**, *13*, 2204154.
- [90] M. Dong, S. Chen, L. Hong, J. Jing, Y. Bai, Y. Liang, C. Zhu, T. Shi, W. Zhong, L. Ying, K. Zhang, *Nano Energy* **2024**, *119*, 109097.
- [91] Y. Thaver, S. O. Oseni, G. T. Mola, *Sol. Energy* **2021**, *214*, 11.
- [92] M. Omrani, H. Fallah, K. L. Choy, M. Abdi-Jalebi, *Sci. Rep.* **2021**, *11*, 19774.
- [93] K. Yao, H. Zhong, Z. Liu, M. Xiong, S. Leng, J. Zhang, Y. X. Xu, W. Wang, L. Zhou, H. Huang, A. K. Y. Jen, *ACS Nano* **2019**, *13*, 5397.
- [94] J. N. Ike, M. S. Hamed, G. T. Mola, *J. Phys. Chem. Solids* **2022**, *161*, 110405.
- [95] S. Ashagre, A. K. Ogundele, J. N. Ike, B. G. Mikael, M. Bekele, G. D. Sharma, G. T. Mola, *J. Phys. Chem. Solids* **2023**, *177*, 111290.
- [96] N. Yang, H. S. Kim, S. Lee, B. Lim, A. C. Grimsdale, D. Ryu, C. E. Song, D. H. Hwang, *ACS Appl. Energy Mater.* **2023**, *6*, 1946.
- [97] K. Zuo, T. Dai, Q. Guo, Z. Wang, M. Du, H. Wang, A. Tang, E. Zhou, Q. Guo, Y. Zhang, *ACS Appl. Energy Mater.* **2022**, *5*, 14271.
- [98] L. Yang, H. Wang, J. Cao, F. Du, J. Yu, W. Tang, *Chem. Eng. J.* **2022**, *427*, 131942.
- [99] J. Hai, L. Li, Y. Song, X. Liu, X. Shi, Z. Wang, X. Chen, Z. Lu, X. Li, Y. Pang, J. Yu, *Chem. Eng. J.* **2023**, *462*, 142178.
- [100] G. Li, L. W. Feng, S. Mukherjee, L. O. Jones, R. M. Jacobberger, W. Huang, R. M. Young, R. M. Pankow, W. Zhu, N. Lu, K. L. Kohlstedt, *Energy Environ. Sci.* **2022**, *15*, 645.
- [101] L. Wang, Q. An, L. Yan, H. R. Bai, M. Jiang, A. Mahmood, C. Yang, H. Zhi, J. L. Wang, *Energy Environ. Sci.* **2022**, *15*, 320.
- [102] X. Li, A. Tang, Q. Guo, X. Guo, J. Chen, Q. Guo, M. Ji, Y. Meng, X. Li, E. Zhou, *ACS Appl. Mater. Interfaces* **2022**, *14*, 32308.
- [103] J. Wen, H. Lin, X. Yu, M. Li, X. Du, J. Luo, G. Yang, C. Zheng, S. Tao, *ACS Appl. Energy Mater.* **2022**, *5*, 12809.
- [104] C. Shang, S. Zhang, D. Han, X. Ding, Y. Zhang, C. Yang, J. Ding, X. Bao, *ACS Appl. Mater. Interfaces* **2023**, *15*, 5538.
- [105] M. L. Keshtov, A. R. Khokhlov, D. Y. Shikin, V. Alekseev, G. Chayal, H. Dahiya, M. K. Singh, F. C. Chen, G. D. Sharma, *ACS Omega* **2023**, *8*, 1989.
- [106] H. E. Wang, Z. Liu, *Org. Electron.* **2022**, *103*, 106465.
- [107] K. N. Zhang, Z. N. Jiang, T. Wang, J. W. Qiao, L. Feng, C. C. Qin, H. Yin, S. K. So, X. T. Hao, *Nano Energy* **2021**, *79*, 105513.
- [108] C. Liu, Z. Wu, N. Qiu, C. Li, Y. Lu, *ACS Appl. Mater. Interfaces* **2023**, *15*, 9764.
- [109] G. D. Sharma, J. Yang, H. Jiang, C. P. Gros, R. Singhal, H. Xu, *Opt. Mater.* **2021**, *118*, 111217.
- [110] K. Wang, H. Wang, G. Li, Y. Hu, X. Guo, M. Zhang, Y. Li, *Chem. Eng. J.* **2021**, *425*, 130575.
- [111] D. Han, S. Wen, F. Bi, C. Shang, X. Ding, A. Saparbaev, E. Zakhidov, V. Kuvondikov, C. Yang, M. Sun, *Chem. Eng. J.* **2023**, *463*, 142400.
- [112] Y. Zhang, J. Deng, Q. Mao, S. Y. Jeong, X. Huang, L. Zhang, B. Lee, B. Huang, H. Y. Woo, C. Yang, J. Xu, *Chem. Eng. J.* **2023**, *457*, 141343.
- [113] X. Xu, Y. Qi, X. Luo, X. Xia, X. Lu, J. Yuan, Y. Zhou, Y. Zou, *Fundam. Res.* **2022**, *3*, 611.
- [114] Q. Wei, S. Liang, W. Liu, Y. Hu, B. Qiu, J. Ren, J. Yuan, F. Huang, Y. Zou, Y. Li, *ACS Energy Lett.* **2022**, *7*, 2373.
- [115] Q. Li, Q. Chen, S. Li, J. Yao, M. Zhang, Q. Wang, C. Zhang, L. Xue, Z. G. Zhang, Q. Yan, *Org. Electron.* **2023**, *114*, 106737.

- [116] L. Yang, J. Qin, S. Li, J. Zhang, Y. Yang, B. Cao, C. He, J. Hou, *Dyes Pigm.* **2022**, *200*, 110147.
- [117] B. Deng, H. Lian, B. Xue, R. Song, S. Chen, Z. Wang, T. Xu, H. Dong, S. Wang, *Small* **2023**, *19*, 2207505.
- [118] R. Peng, Z. Wan, W. Song, T. Yan, Q. Qiao, S. Yang, Z. Ge, M. Wang, *ACS Appl. Mater. Interfaces* **2019**, *11*, 42447.
- [119] J. Wang, H. Yu, C. Hou, J. Zhang, *ACS Appl. Mater. Interfaces* **2020**, *12*, 26543.
- [120] Y. Wang, N. Li, M. Cui, Y. Li, X. Tian, X. Xu, Q. Rong, D. Yuan, G. Zhou, L. Nian, *Org. Electron.* **2021**, *99*, 106305.
- [121] Q. Yang, S. Yu, P. Fu, W. Yu, Y. Liu, X. Liu, Z. Feng, X. Guo, C. Li, *Adv. Funct. Mater.* **2020**, *30*, 1910205.
- [122] M. Zeng, X. Wang, R. Ma, W. Zhu, Y. Li, Z. Chen, J. Zhou, W. Li, T. Liu, Z. He, H. Yan, *Adv. Energy Mater.* **2020**, *10*, 2000743.
- [123] S. Yang, H. Yu, *Chem. Eng. J.* **2023**, *452*, 139658.
- [124] C. Hou, H. Yu, *Chem. Eng. J.* **2021**, *407*, 127192.
- [125] C. Hou, H. Yu, C. Huang, J. Alloys Compd. **2022**, *900*, 163381.
- [126] X. Zhu, B. Guo, J. Fang, T. Zhai, Y. Wang, G. Li, J. Zhang, Z. Wei, S. Duham, X. Guo, M. Zhang, *Org. Electron.* **2019**, *70*, 25.
- [127] X. Huang, H. Yu, S. Shi, C. Huang, *Org. Electron.* **2019**, *65*, 311.
- [128] L. Ma, Y. Xu, Y. Zu, Q. Liao, B. Xu, C. An, S. Zhang, J. Hou, *Sci. China Chem.* **2020**, *63*, 21.
- [129] Z. Hu, Z. Wang, Q. An, F. Zhang, *Sci. Bull.* **2020**, *65*, 131.
- [130] J. Gao, W. Gao, X. Ma, Z. Hu, C. Xu, X. Wang, Q. An, C. Yang, X. Zhang, F. Zhang, *Energy Environ. Sci.* **2020**, *13*, 958.
- [131] N. Sharma, S. K. Gupta, C. M. S. Negi, *Superlattices Microstruct.* **2019**, *135*, 106278.
- [132] L. Zhang, L. Hu, X. Wang, H. Mao, L. Zeng, L. Tan, X. Zhuang, Y. Chen, *Adv. Funct. Mater.* **2022**, *32*, 2202103.
- [133] G. Zhang, D. Hu, H. Tang, H. Song, S. Duan, Z. Kan, S. Lu, *Sol. RRL* **2023**, *7*, 2200994.
- [134] J. Wang, Y. Wang, P. Bi, Z. Chen, J. Qiao, J. Li, W. Wang, Z. Zheng, S. Zhang, X. Hao, J. Hou, *Adv. Mater.* **2023**, *35*, 2301583.
- [135] X. Yang, B. Li, X. Zhang, S. Li, Q. Zhang, L. Yuan, D. H. Ko, W. Ma, J. Yuan, *Adv. Mater.* **2023**, *35*, 2301604.
- [136] X. Song, N. Gasparini, L. Ye, H. Yao, J. Hou, H. Ade, D. Baran, *ACS Energy Lett.* **2018**, *3*, 669.
- [137] L. Liu, J. Chen, Y. Meng, C. Jin, F. Yi, C. Xu, M. Xiao, *Org. Electron.* **2023**, *113*, 106722.
- [138] N. Yao, Q. Fan, Z. Genene, H. Liu, Y. Xia, G. Wen, Y. Yuan, E. Moons, J. van Stam, W. Zhang, X. Lu, *Sol. RRL* **2023**, *7*, 2201134.
- [139] Y. Wang, J. Xue, H. Zhong, C. R. Everett, X. Jiang, M. A. Reus, A. Chumakov, S. V. Roth, M. A. Adedeji, N. Jili, K. Zhou, *Adv. Energy Mater.* **2023**, *13*, 2203496.
- [140] Y. Y. Yu, T. W. Tsai, C. C. Yang, C. P. Chen, *J. Phys. Chem. C* **2017**, *121*, 21969.
- [141] C. Liu, K. Wang, X. Hu, Y. Yang, C. H. Hsu, W. Zhang, S. Xiao, X. Gong, Y. Cao, *ACS Appl. Mater. Interfaces* **2013**, *5*, 12163.
- [142] R. Gui, Y. Liu, Z. Chen, T. Wang, T. Chen, R. Shi, K. Zhang, W. Qin, L. Ye, X. Hao, H. Yin, *Small Methods* **2022**, *6*, 2101548.
- [143] Z. Li, W. Zhong, L. Ying, F. Liu, N. Li, F. Huang, Y. Cao, *Nano Energy* **2019**, *64*, 103931.
- [144] S. Seo, J. W. Lee, D. J. Kim, D. Lee, T. N. L. Phan, J. Park, Z. Tan, S. Cho, T. S. Kim, B. J. Kim, *Adv. Mater.* **2023**, *35*, 2300230.
- [145] Z. Xiao, K. Sun, J. Subbiah, T. Qin, S. Lu, B. Purushothaman, D. J. Jones, A. B. Holmes, W. W. Wong, *Polym. Chem.* **2015**, *6*, 2312.
- [146] X. Lin, S. Tu, L. Xiao, H. Zhen, W. Wang, Q. Ling, *Chem. Eng. J.* **2023**, *464*, 142634.
- [147] J. Choi, W. Kim, S. Kim, T. S. Kim, B. J. Kim, *Chem. Mater.* **2019**, *31*, 9057.
- [148] H. Mao, L. Zhang, L. Wen, L. Huang, L. Tan, Y. Chen, *Adv. Funct. Mater.* **2023**, *33*, 2209152.
- [149] L. Zhu, M. Zhang, G. Zhou, T. Hao, J. Xu, J. Wang, C. Qiu, N. Prine, J. Ali, W. Feng, X. Gu, *Adv. Energy Mater.* **2020**, *10*, 1904234.
- [150] G. Feng, J. Li, Y. He, W. Zheng, J. Wang, C. Li, Z. Tang, A. Osvet, N. Li, C. J. Brabec, Y. Yi, *Joule* **2019**, *3*, 1765.
- [151] Y. Zhang, Z. Liang, J. He, W. Ni, M. Li, Y. Geng, *Dyes Pigm.* **2022**, *202*, 110269.
- [152] L. Duan, Y. Zhang, H. Yi, F. Haque, C. Xu, S. Wang, A. Uddin, *Mater. Sci. Semicond. Process* **2020**, *105*, 104750.
- [153] X. Cheng, M. Li, Z. Liang, M. Gao, L. Ye, Y. Geng, *ACS Appl. Energy Mater.* **2021**, *4*, 8442.
- [154] L. Wang, L. Zhang, S. Kim, T. Wang, Z. Yuan, C. Yang, Y. Hu, X. Zhao, Y. Chen, *Small* **2023**, *19*, 2206607.
- [155] Z. Li, Y. Liang, L. Chen, J. Chen, F. Peng, L. Ying, *Chem. Eng. J.* **2023**, *452*, 139228.
- [156] F. Qi, Y. Li, R. Zhang, F. R. Lin, K. Liu, Q. Fan, A. K. Y. Jen, *Angew. Chem. Int. Ed.* **2023**, *62*, e202303066.
- [157] J. Chen, J. Cao, L. Liu, L. Xie, H. Zhou, J. Zhang, K. Zhang, M. Xiao, F. Huang, *Adv. Funct. Mater.* **2022**, *32*, 2200629.
- [158] D. Sun, W. Tang, J. Guo, J. Wang, Z. Ding, R. Hao, M. Zhu, Y. Liu, X. Song, W. Zhu, *ACS Appl. Energy Mater.* **2022**, *5*, 15423.
- [159] H. Tan, B. Yuan, Z. Shao, W. Deng, J. Yu, M. Xiao, H. Wu, W. Zhu, *Chem. Eng. J.* **2022**, *445*, 136691.
- [160] T. Yu, W. He, M. Jafari, T. Guner, P. Li, M. Siaj, R. Izquierdo, B. Sun, G. C. Welch, A. Yurtsever, D. Ma, *Small Methods* **2022**, *6*, 2100916.
- [161] Q. Fan, R. Ma, Z. Bi, X. Liao, B. Wu, S. Zhang, W. Su, J. Fang, C. Zhao, C. Yan, K. Chen, *Adv. Funct. Mater.* **2023**, *33*, 2211385.
- [162] Z. Chen, J. Zhu, D. Yang, W. Song, J. Shi, J. Ge, Y. Guo, X. Tong, F. Chen, Z. Ge, *Energy Environ. Sci.* **2023**, *16*, 3119.
- [163] Y. Cui, Z. Chen, P. Zhu, W. Ma, H. Zhu, X. Liao, Y. Chen, *Sci. China Chem.* **2023**, *66*, 1179.
- [164] H. Chen, S. Y. Jeong, J. Tian, Y. Zhang, D. R. Naphade, M. Alsufyani, W. Zhang, S. Griggs, H. Hu, S. Barlow, H. Y. Woo, *Energy Environ. Sci.* **2023**, *16*, 1062.
- [165] R. Ma, H. Li, T. A. D. Peña, X. Xie, P. W. K. Fong, Q. Wei, C. Yan, J. Wu, P. Cheng, M. Li, G. Li, *Adv. Mater.* **2023**, 2304632, <https://doi.org/10.1002/adma.202304632>.
- [166] Z. Yin, S. Mei, L. Chen, P. Gu, J. Huang, X. Li, H. Q. Wang, W. Song, *Org. Electron.* **2021**, *99*, 106308.
- [167] M. Xiong, J. Wu, Q. Fan, Q. Liu, J. Lv, X. Ou, X. Guo, M. Zhang, *Org. Electron.* **2021**, *96*, 106227.
- [168] N. Gasparini, S. H. K. Paletti, J. Bertrandie, G. Cai, G. Zhang, A. Wadsworth, X. Lu, H. L. Yip, I. McCulloch, D. Baran, *ACS Energy Lett.* **2020**, *5*, 1371.



Morongwa E. Ramoroka received his Ph.D. degree in chemistry from the Department of Chemistry, University of the Western Cape, South Africa in 2022. Currently, he is a postdoctoral researcher fellow at the Department of Chemistry, University of Cape Town, South Africa. The research expertise of Dr Ramoroka is in the area of functional polymeric materials for solar cell applications. He was awarded a junior researcher fellowship under the European Union H2020 RISE (2017) INFINITE-CELL-DVL-777968 project for research exchange visit to Helmholtz Zentrum Berlin, Germany.



Sodiq T. Yussuf is a lecturer in the Department of Chemical Sciences, Olabisi Onabanjo University (OOU), Nigeria. He holds a B.Sc. in industrial chemistry (2008, OOU), an M.Sc. in industrial chemistry (2012, University of Ibadan, Nigeria), and a Ph.D. in chemistry (2021, University of the Western Cape, South Africa) degrees. His research focuses on the synthesis and characterization and thin film solar cell applications of novel kesterite materials. His awards include the Junior Researcher Fellowship Award within the EU Horizon 2020 RISE (2017) INFINITE-CELL-DVL-777968UAB Project, for secondment to the UAB Modernios E-Technologijos (MET), Vilnius, Lithuania in 2019.



Kelechi C. Nwambaekwe's expertise involves the use of inner transition metals to design nanomaterials for solar cell applications. He obtained his Ph.D. (2023) degree in chemistry from the University of the Western Cape (UWC), South Africa. Presently, he is a DSI-NRF Postdoctoral Innovation Fellow at UWC for research on high-efficiency tandem solar cells. His awards include a Junior Researcher Fellowship under the European Union H2020 RISE (2017) INFINITE-CELL-DVL-777968 project for research exchange to the Institute of Applied Physics, Chisinau, Moldova in 2019 and the University of Granada, Spain, Erasmus+ KA107 International Dimension Programme Fellowship (2023).



Kwena D. Modibane is an associate professor of chemistry at the University of Limpopo (UL), South Africa, the DSI-NRF South African Research Chair Initiative (SARCHI) chair for Photoelectrocatalytic Hydrogen Production, and the leader of the Nanotechnology Research Group at the University of Limpopo (NanoRG@UL). His current research interest involves the designing and production of specialized composite materials for hydrogen storage, solar cells, supercapacitor, and water treatment applications. He is a recipient of the 2019 University of Limpopo Vice Chancellor's Established Researcher Award.



Vivian S. John-Denk obtained her doctoral training at the University of the Western Cape (UWC), South Africa and the Linz Institute for Organic Solar Cells ((LIOS)), Johannes Kepler University of Linz, Austria. Her qualifications include B.Sc. (Hons.) in industrial chemistry (2009, Ekiti State University, Nigeria), M.Sc. in chemistry (2013, University of Johannesburg, Johannesburg, South Africa), and Ph.D. in chemistry (2017, UWC). She was awarded a Coimbra Group Scholarship for Young Professors and Researchers from sub-Saharan Africa and South Africa (for exchange to the University of Padova, Italy in 2014), and the ICTP-ANSOLE Africa-North Exchange Program Fellowship - hosted by LIOS in 2015.



Samantha F. Douman obtained her B.Sc. and Ph.D. degrees in chemistry from the University of the Western Cape, South Africa and Dublin City University, Ireland, respectively. She is currently a lecturer at the Department of Chemistry, University of Cape Town, South Africa. Her research interests are largely directed toward the exploitation of material science (nanomaterials, polymers, etc.) in the development of next-generation electrochemical sensor technologies for targets of biological, chemical, and environmental origins. Her recent awards include the Department of Science and Innovation-National Research Foundation (DSI-NRF) Innovation Postdoctoral Fellowship Award (2019–2021).



Emmanuel I. Iwuoha is a professor of chemistry, the South African (SA) Research Chair for NanoElectrochemistry and Sensor Technology and the Founder and Director (since 2002) of the University of the Western Cape Sensor Laboratories (SensorLab)—a center of excellence for electrochemistry in Africa. His research work focuses on the creation of smart functional nanomaterials for electroanalytical sensor and electrochemical energy applications. His recent awards and recognitions include SA National Research Foundation (NRF) A-Rated Scientist Award 2019, Honorary Fellow of the Royal Society of Chemistry (*HonFRSC*) UK Award 2021 and Fellow of the Royal Society of South Africa (*FRSSAf*) 2023.